Conceptual Design and Instrumentation Study
For a 2-D, Linear, Wet Steam Turbine Cascade Facility

By

Jacob Andrew McFarland

Thesis submitted to the faculty of the Virginia Polytechnic Institute and State University in partial fulfillment of the requirements for the degree of

Master of Science
In
Mechanical Engineering

Approved by:

Dr. Wing F. Ng Committee Chair
Dr. Francine Battaglia
Dr. Al K. Kornhauser

December 4th, 2008
Blacksburg, Virginia

Keywords: Steam Turbines, Steam Cascade, Wet Steam, Nucleation, Condensation, Instrumentation,

Contains Proprietary Information

Conceptual Design and Instrumentation Study
For a 2-D, Linear, Wet Steam Turbine Cascade Facility

Jacob Andrew McFarland

Abstract

The design of last stage low pressure steam (LP) turbines has become increasingly complicated as turbine manufacturers have pushed for larger and more efficient turbines. The tip sections of these LP turbines encounter condensing wet steam at high velocities resulting in increased losses. These losses are difficult to predict with computational fluid dynamic models. To study these losses and improve the design of LP turbines a study was commissioned to determine the feasibility and cost of a steam cascade facility for measuring low pressure turbine blade tip section aerodynamic and thermodynamic performance.

This study focused on two objectives: 1) design a steam production facility capable of simulating actual LP turbine operating conditions, and 2) design an instrumentation system to measure blade performance in wet steam. The steam production facility was designed to allow the test section size to be selected later. A computer code was developed to model the facility cycle and provide equipment requirements. Equipment to meet these requirements, vendors to provide it, and costs were found for a range of test section sizes. A method to control the test section conditions was also developed.

To design the instrumentation system two methods of measuring blade losses through entropy generation were proposed. The first method uses existing total pressure probe techniques. The second method uses advanced particle imaging velocimetry techniques possibly for the first time in wet steam. A new method is then proposed to modify the two techniques to take measurements at non-equilibrium states. Finally accuracy issues are discussed and the challenges associated with achieving periodic flow in this facility are investigated.

Acknowledgements

I would like to first thank my family and my fiancée, Tiffany, for their continued support through out my graduate education. Without their help I could not have survived my first semester. I would also like to thank my mother and fiancée for proof reading my thesis.

I would also like to acknowledge my friends and officemates who helped me to enjoy my time at Virginia Tech and blow off stress. Clayton De Losier my officemate provided me with a distraction when ever one was needed, Jonathan McGlumphy kindly shared with me his years of experience as a graduate student, and Kat Tran gave me friendship and a familiar face in nearly every class I took.

The work for this thesis was done at Techsburg Inc. and I am indebt to them for their help. I would like to thank Sandra Gunter for her help with my many computer problems, and Stephen Guillot for providing the CFD models used in this paper and for his guidance and mentoring.

This project was funded by the General Electric Company and I am extremely grateful for their funding and support. I would like to thank Doug Hofer, Tao Guo, and Jon Slepski, of GE who supported my work and provided advice.

I would like to thank Dr. Wing Ng my advisor for his in depth help in the writing of this thesis and his guidance throughout my graduate education. I also owe Dr. Al Kornhauser for his advice early in this project and for proving me with the Matlab steam table functions I used extensively throughout this project. I am thankful also to both Dr. Kornhauser and Dr. Francine Battaglia for serving on my committee and providing their support.

Table of Contents

Table of Figures

Table of Tables

Nomenclature

Variables

d	Droplet diameter
f	Function of
ΔG^*	Free-energy barrier
h	Enthalpy
J_{cl}	Nucleation rate
k	Boltzmann constant
Kn	Knudsen number
m	Mass
m_w	Mass of water molecule
p	Pressure
S	Saturation Pressure Ratio
s	Entropy
q_c	Condensation Coefficient
r	Droplet Radius
R	Gas Constant for H2O
t	Time
T	Temperature
ΔT	Super Cooling
TW	Turbine Work Extraction
v	Velocity
x	Wetness
y	Dryness
ρ	Density
σ	Surface Tension for H2O
μ	Viscosity for H2O

Subscripts and Superscripts

cap	Capillary value
err	Value with error
l	Liquid phase
v	Vapor phase
s	Saturation value
t	Turbine inlet
ts	Test section inlet
I	Inertial relation
fg	Liquid/vapor phase difference
$*$	Critical size
0	Total quantity
$\bullet$	Rate (quantity per time)

1.0 Introduction

The large majority of electric power in the world is produced from steam turbines. In large steam power plants, steam is run through a high pressure (HP), an intermediate pressure (IP), and multiple low pressure (LP) steam turbines before being exhausted to the condenser. In order to maximize the power extraction the steam must be cooled into the saturation dome where it becomes wet steam. The steam pressure must also be lowered, decreasing the density of the steam and resulting in a much larger volumetric flow rate. This larger flow rate is handled by dividing the flow between multiple LP steam turbines and by increasing the exit diameter of these turbines. Larger diameter last stage steam turbines allow improved cycle efficiency and reduce power plant operating costs. These large turbines encounter near sonic inlet and supersonic exit velocities at their tip sections. At these velocities, predicting the behavior of wet steam is very difficult. Rapid nucleation occurs in the tip sections resulting in much larger losses than are experienced in earlier stages of the turbine train. Reducing these losses and improving the turbine train efficiency by small amounts can result in large profit gains for both turbine manufacturers and power producers.

While some computational fluid dynamics (CFD) codes have attempted to predict the behavior of wet steam in LP turbine stages, additional experimental verification is still needed. Testing of LP steam turbine blades has often been carried out in air tunnels. These tests offer verification of the aerodynamic performance but do not account for the effects of condensation on the blade aerodynamics or the thermodynamic losses associated with phase change that occurs in wet stages. Testing in wet steam is advantageous because both the aerodynamic losses and the thermodynamic losses can be

found accurately. For this reason, the General Electric Company (GE) commissioned a study to evaluate the feasibility and cost of producing a facility to test their LP turbine blade tip section designs in wet steam. From this study, the proposed GE steam cascade facility discussed in this paper has been designed and is proposed for construction.

There were two major objectives identified in designing the GE steam cascade facility: 1) design a steam production facility (Chapter 2), and 2) design a system for measuring the blade performance (Chapter 3). To complete the first objective, the steam production facility was designed with two variations that will cover the range of expected test section sizes where the final size will be determined later. The steam production facility was also designed to be capable of providing steam for a range of test section conditions and to minimize both steam production and operating costs. Equipment to meet the design specifications and vendors to provide it were found. Finally, to complete the facility design, a system of control capable of reaching various test section conditions was developed. To complete the second objective, methods to measure blade performance were created, and the measurements required were determined. Instrumentation to take these measurements in wet steam was identified. To improve the accuracy of blade performance measurement, a method to take measurements in non-equilibrium steam was also created. Finally instrumentation accuracy and periodicity issues were addressed.

2.0 Steam Production Facility Design

The major difference between the proposed GE steam facility and typical wind tunnels is the need to produce steam. A steam production facility requires a greater amount of engineering and design than typical wind tunnels. The problems encountered in this steam production facility required original solutions. To describe the steam production facility design, previous steam facilities similar to the proposed GE steam facility found in literature are reported first. Next, the test section conditions required for modeling the full scale turbine tip sections are discussed. Cycle options and the cycle chosen are described. Equipment to meet these requirements and the test section design are then described. Finally, a method for control of the test section conditions is explained.

2.1 Previous Wet Steam Turbine Testing Facilities

While the main purpose of the proposed GE steam facility is to provide direct measurement of losses for turbine blades, most existing steam cascade facilities were designed to test nucleation theories. The proposed GE steam facility is very similar to these and could also be used for research on condensation models and nucleation theory. The GE steam facility's design drew upon the knowledge gained in these existing facilities, and a brief discussion of their design is necessary to understand the design of the proposed GE steam facility.

The most similar facility found in existing literature is the former Central Electricity Research Laboratory (CERL) located in Leatherhead, England. This facility was originally built to test the erosion effects of water droplets and is described by Christie and Hayward [1]. The CERL has been used for many publications, and

additional information on its design and various capabilities can be found in the works of Moore et al. [2], Skillings [3], and White et al. [4]. This facility was a closed-loop cycle using a single stage impulse turbine to create accurately sized droplets in the test section. It relied on two boilers for steam generation and a condenser to provide the required back pressure on the test section. This facility was capable of continuous operation at approximately 36,000 lbm/hr mass flow with a test section inlet area of approximately 12 in by 6 in, making it similar in size to the proposed GE steam facility.

Another important wet steam facility is housed at the University of Birmingham, England. This facility was constructed for the purpose of verifying nucleation theory. Descriptions of its design can be found in the publications of Bakhtar et al. [5-8]. This facility is a blow-down type capable of 700 ms of quasi-steady flow. Water droplets are created by the expansion of super-cooled steam from the receiver tank through a converging/diverging nozzle. Droplet sizes can be changed by using different nozzles with varying expansion rates. The advantage of this facility is that it has the ability to produce accurate wet steam conditions without the added costs of a turbine and the expense of running a continuous cycle. The disadvantage is that measurements must be made in less than 700 ms, and adjustments must be made between tests.

Other important facilities found in literature were that of Ikeda and Suzuki [9] and Parvizinia et al. [10]. These two facilities provided little information on their construction and design but are interesting for comparison to the proposed GE steam facility. The facility used by Ikeda took a unique approach by using steam generated by an existing electric power plant. This method of steam generation will reduce the cost of a steam cascade facility but provides additional complications in conditioning the steam.

Droplets were created in this facility by atomizing nozzles which produce sizes far greater than those seen in turbines. The Ikeda facility was constructed in 1976 and has been demolished. The Siemens Power Generation Flow Lab facility in Mulheim, Germany described by Parvizinia is a closed-loop cycle that uses a boiler and condenser for steam generation, runs in continuous operation, and has a cascade geometry similar to the proposed GE steam facility design. The Siemens facility contains many interesting test section features such as porous inlet guide walls and a large open jet exit. It is unknown whether this facility was designed for wet inlet conditions, and there is no evidence of a turbine or other method for generating water droplets. This facility may be very similar to the proposed GE steam facility, but very little information about it is available in published literature. This lack of information is most likely due to the competitive nature of the steam turbine market.

2.2 Test section conditions

The first step in designing the steam production facility was to determine the design requirements from the test section conditions. The proposed GE steam facility was designed to test a blade tip section of a last stage rotor in a GE low pressure condensing steam turbine with an 85 inch diameter and an operating speed of 3000 rpm. The tip section is being tested due to its high expansion rate where condensation is complicated by non-equilibrium effects (Section 3.1) and the accuracy of CFD models is poor. The mass flow, pressure, and wetness vary over the operating range of this turbine, producing blade Reynolds numbers from 200,000 to 600,000, based on the true chord and exit conditions. The turbine tip section operating conditions for a blade Reynolds number of 600,000 are listed in Table 1.

Inlet Mach #	0.95
Inlet Wetness	4%
Inlet Angle	82°
Exit Mach #	1.85
P01/P2	7.5
Angle	72°
Pitch	8"
True Chord	8.23”

Table 1: Blade Tip Section Conditions

The actual turbine blades of the GE LP turbine are 3-D in shape and contain twist, tapper, and varying 2-D airfoil shapes, as you move from the shaft outwards to the tip. To determine the performance of these 3-D blades, the performance of their 2-D blade sections must be determined. For the GE steam facility The 2-D tip sections will be tested for the GE steam facility. Data from these 2-D sections can be used to improve the performance of the 3-D blade design. These 2-D blade sections operate in an annular, rotating turbine rotor. To acquire data from these sections, they will need to be stationary. The flow conditions these blade sections experience in a rotating reference frame will be reproduced in a stationary reference frame. In the actual turbine, the blade section are mounted in an annular pattern. While this can be reproduced in a stationary annular cascade, but these cascades are very large and expensive. These blade sections can also be mounted in a stationary linear cascade where the tangential arrangement of the blade sections are unwrapped into a linear arrangement. This linear arrangement of the 2-D blade sections will create a 2-D flow field around the blade sections without interference from 3-D effects experienced in the actual turbine. To determine the performance of the GE LP turbine blade tip section, the section will be tested in a stationary, 2-D linear cascade.

Understanding the characteristics of the 2-D flow field around these blade sections will be necessary to understand the facility design challenges unique to the GE LP turbine tip section geometry. The flow field around this blade section is characterized by the high subsonic inlet velocities and supersonic exit velocities. If the inlet velocity increases by a small amount the inlet velocity can become supersonic and inlet bow shocks (Figure 1) will develop which will restore the steam speed to subsonic velocities before entering the blade passage. As steam enters the blade passage it will be accelerated to Mach one at the blade throat. After the blade throat the steam will be expanded to supersonic velocities in the remainder of that blade passage and continue to expand in the exit flow field. The supersonic velocities at the blade passage exit will cause fishtail shocks to form from the pressure and suction sides of the blade trailing edge. In between these fishtail shocks an area of much slower flow with high losses will develop known as the wake. The position of the fishtail shocks can interfere with the establishment of periodic flow conditions as explained in Section 3.8.

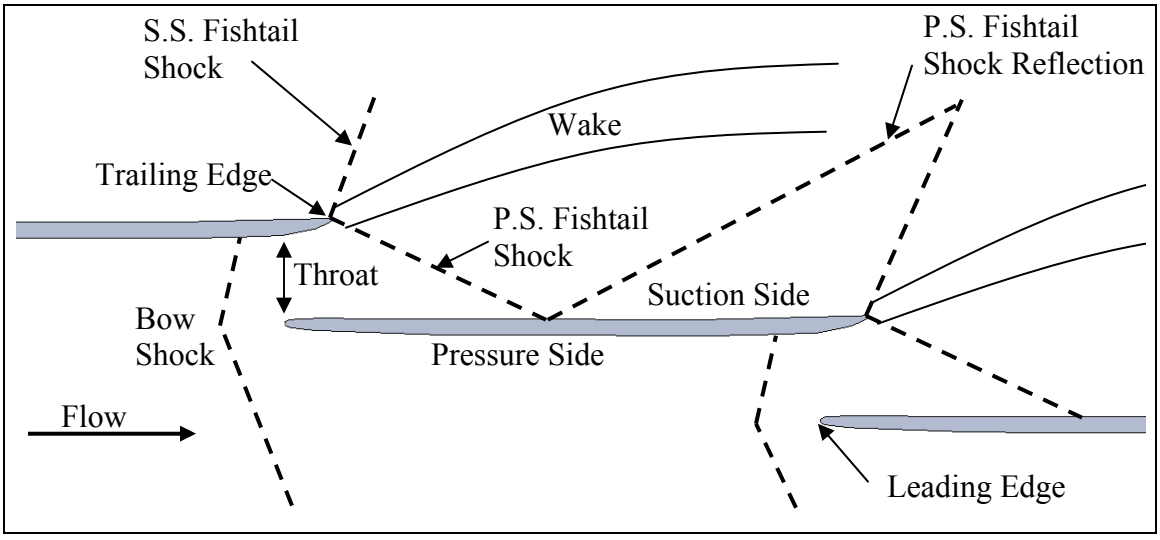

Figure 1: Flow Field Conditions

The size required for this cascade is driven by the need to establish periodic flow conditions. A separate project was initiated to determine the size of the test section needed. In this project, the blade section was tested in an air cascade tunnel with various shockwave reflection cancellation methods and various configurations of aspect ratio (blade span / chord length) and number of blade passages. The results from this project have not been finalized, but preliminary results from this project can be found in Appendix E. Before these preliminary results were available, it was assumed a larger test section size with 12 blade passages, an aspect ratio of 1.5, and a scale (test blade dimensions / actual blade dimensions) of 0.5 would be needed to establish 2-D, periodic flow. The preliminary results of the air cascade project showed a smaller test section size could be used with 8 passages, an aspect ratio of 0.75, and a scale of 0.5. These two cascade sizes were used as upper and lower bounds for the expected test section size, which intern required two steam production facility size variations. The test section size will be finalized upon completion of the air cascade project and is beyond the scope of this thesis. For this reason, two variations on the steam production facility design were made to allow flexibility for the test section size that will be determined later.

Both test section sizes use a blade scale of 0.5 to reduce the size of the cascade. The scale could not be reduced any further without exceeding the limits of production methods. Scale will affect the Reynolds number and test section intensive properties, while the number of passages and aspect ratio will only affect the required mass flow, and other mass flow dependent extensive properties. These test section extensive properties were normalized by the cascade throat area so that they apply to any size test section with a 0.5 scale. The cascade throat area was determined by multiplying the inlet

area (total pitchwise length times the span) by 1.002, the A/A* value corresponding to the inlet Mach number. With the test section properties normalized, the solution for one test section size can be used to find the test section properties at a given Reynolds number for any number of passages or aspect ratio.

Having normalized the properties of the test section, solutions for blade exit Reynolds numbers from 200,000 to 600,000 were found using the Matlab code describe in Section 2.3. To vary the Reynolds number in the cascade test section and meet a target inlet wetness, the density, pressure, and mass flow must be varied. The facility will need to provide 120 $\left(lbm/hr \cdot in^2\right)$ of 4% wet steam to the test section at a pressure of 8 psia to reach the highest required Reynolds number. To achieve an exit Mach number of 1.85, the required test section back pressure is 7 psia and local test section pressure will reach as low as 1.5 psia. The mass flow will need to be reduced 30 lbm/(hr*in^2) to achieve a Reynolds number of 200,000.

2.3 Cycle selection

The GE steam facility needs to be capable of providing the test section conditions continuously in order to provide the best access to measurements. A closed cycle was selected to meet this need, although many different cycles were considered. A Quasi-Brayton cycle using a steam compressor would provide significantly reduced operating costs by eliminating the need to condense and boil the steam. However, a compressor capable of handling saturated steam was necessary to close this cycle and could not be found from any manufacturer. For this reason, a Quasi-Rankine cycle with a boiler and condenser that utilizes pre-manufactured equipment was selected. A turbine was added to the cycle to generate accurately sized water droplets at the test section inlet. A detailed

explanation of the selection of this cycle versus other options can be found in Appendix B.

A basic Matlab [11] code was developed to select the equipment necessary for the cycle using steam properties and the conservation of mass, momentum, and energy equations. The steam properties were provided by Matlab functions based on the International Association for the Properties of Water and Steam (IAWPS) formulation 1995, and written by Dr. Al Kornhauser of Virginia Tech [12]. The code is capable of providing the thermodynamic state at inlet and exit of every major piece of equipment for a given test section Reynolds number using some assumptions about the equipment performance. The first assumption made was that the steam circuit, including the equipment, would be adiabatic. To model the test section, it was assumed that the steam flow would undergo a normal shockwave at the exit of the blade row. In reality, many oblique shocks will occur at the cascade exit which decelerate the flow more isentropically, but modeling a normal shock is simpler and provides the worst-case scenario. Diffusion to sub-sonic speeds after the oblique shocks may also be highly non-isentropic, making the normal shock model more realistic.

Modeling the normal shock in two-phase flow required using the separated flows model described by Moore and Sieverding [13] and Johnson [14]. The separated flow model predicts the two-phase steam conditions after a shockwave by treating the water and steam masses as separate fluids that undergo separate processes. The two phases are assumed to initially be in thermodynamic and inertial equilibrium (Section 3.1 and 3.3). The steam will undergo a shock as if no water is present while the water will remain unchanged. The steam shock was modeled using the basic conservation equations rather

than ideal gas shock equations. After the shock wave, the flows were combined to find an equilibrium state using the conservation equations.

Assumptions about the equipment were also needed for the Matlab program to solve for the steam cycle equipment conditions. The boiler and the condenser were assumed to experience no pressure drop across them. The quality at exit to the boiler and condenser were also assumed to be 0% and 100% wet, respectively. The turbine and pump were calculated using an assumed isentropic efficiency of 50 and 90 percent respectively. Using the required test section inlet and outlet conditions and these assumptions, the states at inlet and outlet of each piece of equipment could be found with simple thermodynamic functions and the basic conservation equations. A simple diagram of the Matlab program cycle is shown in Figure 2.

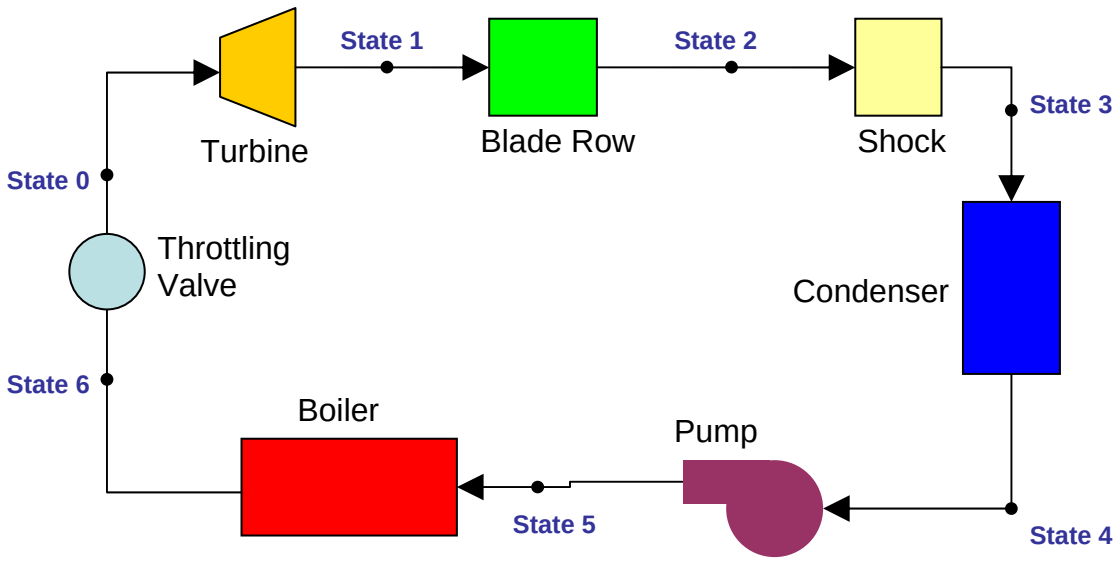

Figure 2: Steam Cycle

2.4 Equipment Selection

Once the Matlab code was completed, equipment could be selected to match the calculated conditions. The steam generating equipment was selected first because it

determines the largest part of energy input required for the cycle. Conventional industrial boilers will be used to produce steam. These boilers are designed to produce saturated steam, so a throttling valve will be used to superheat the steam before entering the turbine. By throttling the steam, the pressure and temperature will be reduced in a way that moves the steam away from saturation and superheats it. This requires that the boiler pressures be higher than the turbine inlet pressure. Calculations from the Matlab code showed that for the larger test section size discussed in section 2.2, the boiler pressures would need to reach a maximum of approximately 55 psia. Standard 150 psig rated boilers were chosen because they are the lowest pressure rated boilers that will accommodate the required 55 psia pressure.

A single boiler could be used to produce the required mass flow for either test section size, but multiple boilers were used for the larger test section size to maximize the turndown ratio and minimize the power consumption during idle. The selection of multiple boilers may also be necessary to comply with governmental environmental regulations depending on the test section size selected. Water-tube boilers were chosen over more common fire-tube boilers due to their quicker response to changing loads. The number and type of boilers needed for various test section sizes can be found in Figure 3, and their costs can be found in Table 2.

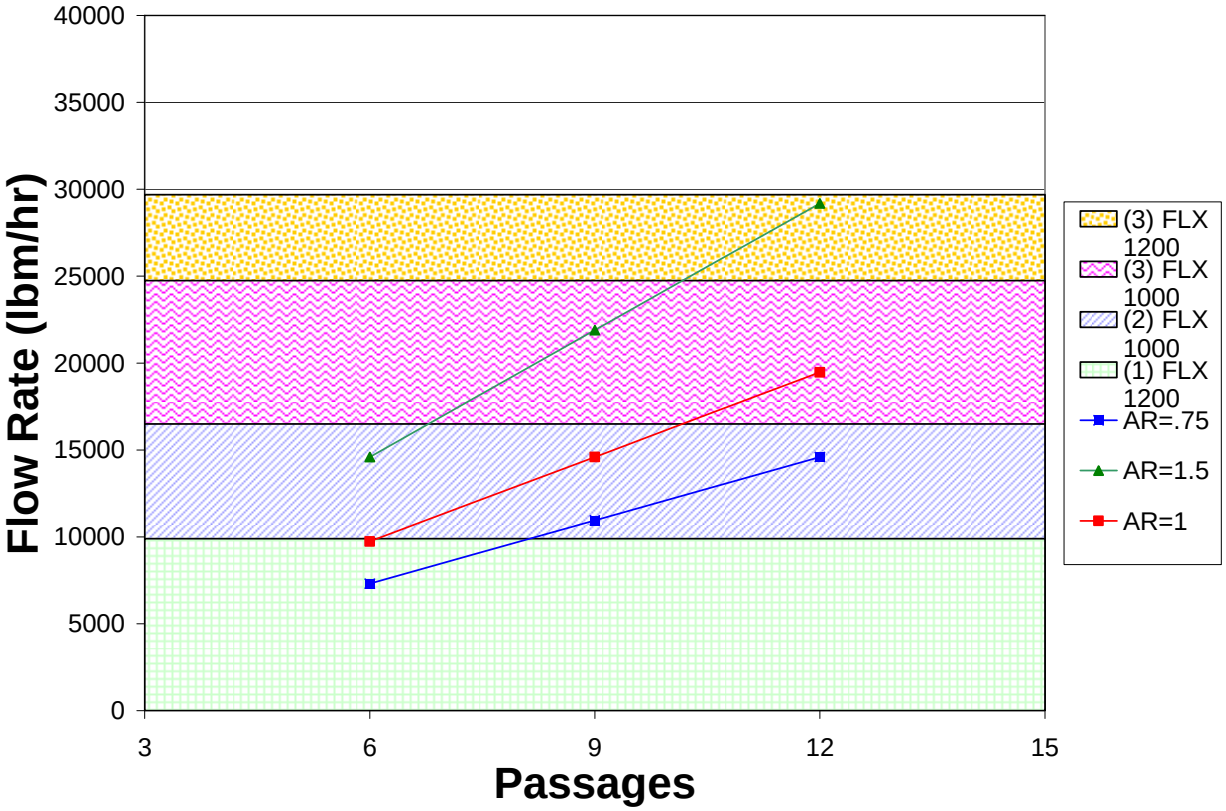

Figure 3: Boiler Capabilities vs. Test Section Size

Qty	Maker	Model	Est. Cost
3	Cleaver Brooks	FLX 1200	$456,000
3	Cleaver Brooks	FLX 1000	$376,000
2	Cleaver Brooks	FLX 1000	$250,000
1	Cleaver Brooks	FLX 1200	$200,000

Table 2: Estimated Cost for Various Boilers

Additional components included in the steam generating equipment are a deaerator, surge tanks, water treatment, and pumps. The deaerator and water treatment are essential to remove oxygen and other foreign particles from the steam and make-up

water. Because the equipment will be operated below atmospheric pressure in most areas, some air is expected to leak into the system. It is also expected that air will enter from the purging system of the test section pressure transducers. Air needs to be removed from the system to ensure that the nucleation process is unaffected. The deaerator removes air through the use of high-pressure steam extracted at the boiler exit. This steam is bubbled through the water phase before it enters the boilers, entraining air particles and removing them with a small amount of vented steam. Chemicals added during the water treatment also serve to remove air from the system and prevent oxidation of equipment.

Solid particles are likely to be created by the slow erosion of equipment and piping. The use of stainless steel piping and equipment will reduce the amount of solid particles entering the system due to iron oxidation. The presence of high quantities of solid particles will greatly alter the nucleation rate in the test section. At start-up, particles and air can be removed from the test section by means of a blow-down where high-pressure steam is flushed through the test section and vented, taking with it air and solid particles. Solid particles that are trapped in the water drum of the boiler are removed via periodic blow-downs of the water drum.

The condenser system equipment was the next equipment chosen. Some industrial steam applications of similar mass flow to the proposed GE steam facility do not recover steam but instead vent it after all useful work potential has been exhausted. Venting was considered for this cycle but was not feasible due to the sub-atmospheric test section total pressure. The simplest way to provide the required low pressure was to use

a condenser to condense the exhaust steam and provide a sub-atmospheric back pressure to the test section.

Traditional condensers for large scale steam turbines are coupled directly to the low pressure section, but a separated tube and shell heat exchanger, a common design for utility feed water heaters, was selected for the proposed GE steam facility. The tube and shell heat exchanger condenses steam by passing cooling water through U-tube bundles while the condensing steam passes around the bundles on the shell side. Cooling water for the condensers of electric power plants is often provided by means of a cooling pond or cooling towers. A cooling tower was found to be the more economical option for the proposed GE steam facility's size. The cooling tower cools water mostly by evaporation, creating a small increase in water consumption.

The turbine and dynamometer were the final equipment to be selected for the cycle. This small turbine was included in the cycle to provide water droplets of similar size to those produced in actual LP turbines. The turbine will condense the steam properly by extracting enthalpy without heat transfer. Droplets formed in this manner are very numerous and small (<0.50 μm) and closely match those produced in large LP steam turbine stages. The size of the turbine was determined by assuming a five degree inlet superheat to ensure no condensation occurs before the turbine, an isentropic efficiency of 50%, and an exit wetness of nearly 4%. These assumptions yielded a turbine power extraction of approximately 500 hp for the larger test section size and 230 hp for the smaller test section size.

Selecting a turbine of this power was complicated by the very low pressures and relatively high mass flow rate. Two turbines were selected to match the large and small

test section sizes (Table 3). The first of these was a custom made turbine that was sized and quoted by a turbine manufacturer for the larger test section size. This turbine was a two stage turbine, which operated at an isentropic efficiency of 50% and an inlet pressure of 65 psia. For the smaller test section size, a more practical single stage turbine was found with a similar isentropic efficiency but smaller inlet area. The mass flow rate handled by these turbines is limited by their inlet area and inlet pressure. In order to match the required test section conditions, this second turbine will be operated at much lower inlet pressures with a much lower mass flow than the quoted conditions shown in Table 3. The turbines will be operated at different speeds to reduce the efficiency and hp for different test section conditions.

	Large Turbine	**Small Turbine**
Inlet Pressure (psia)	**65**	**140**
Inlet Temperature (F)	**322**	**375**
Exit Pressure (psia)	**12**	**12**
Steam Rate (lbm/hp-hr)	**29.96**	**30.6**
Steam Flow Rate (lbm/hr)	**29,200**	**29,000**
Turbine Speed (rpm)	**5,350**	**3,600**

Table 3: Steam Turbine Specifications

Many options to dissipate the power produced by the turbine were considered, including various ways to reuse the power. A commercial dynamometer was found to be the most economical even though it will not recover any of the power dissipated.

Commercial dynamometers are readily available at the required power, but most are designed to match the power curves of automotive engines. However, some companies produce dynamometers designed for steam and gas turbines. The dynamometer selected was designed to operate on gas turbines and can handle as much as 1000 hp at speeds up to 10,000 rpm. This dynamometer uses a water brake and requires cooling water to dissipate the power from the turbine in the form of heat. This cooling water will be provided by the cooling tower. A process diagram for the equipment selected is shown in Figure 4.

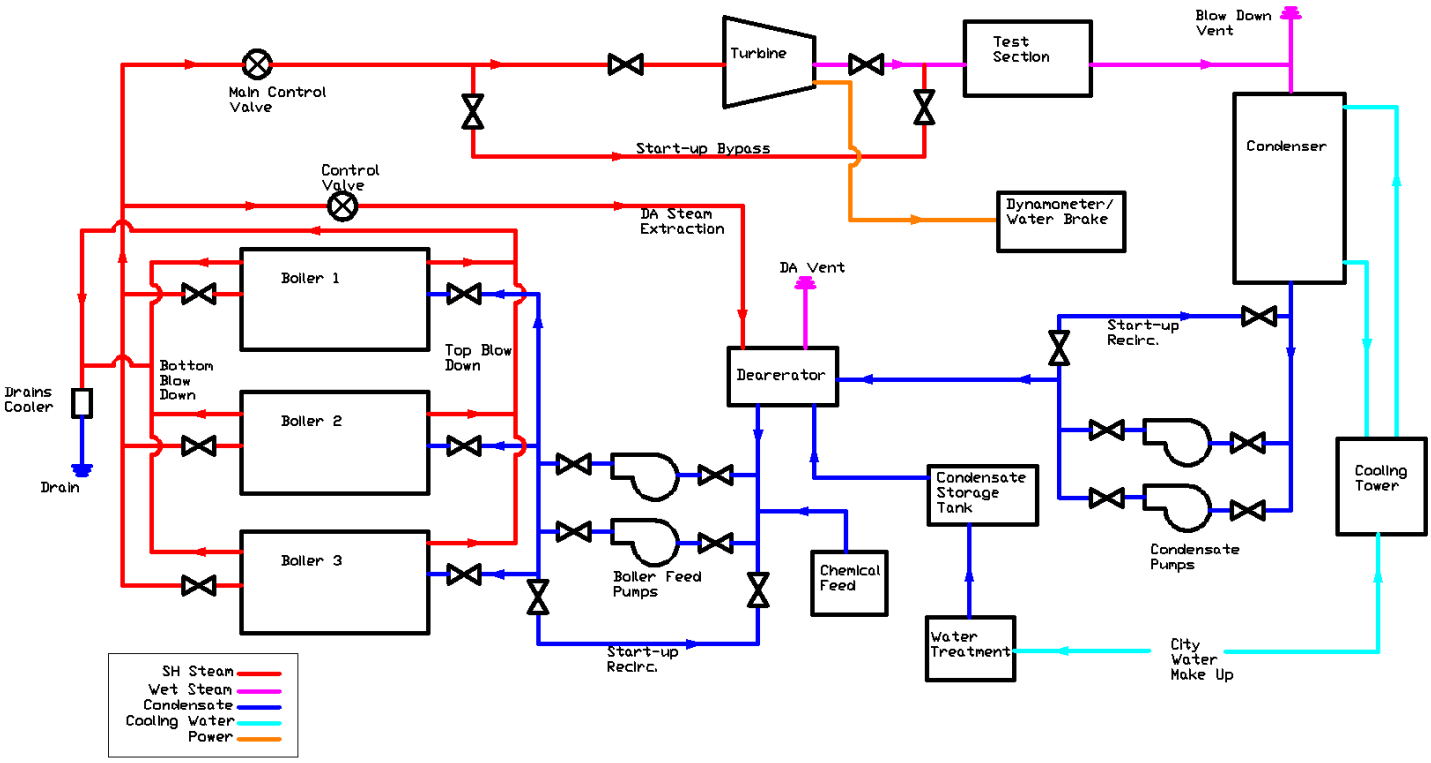

Figure 4: Process Diagram

2.5 Test Section Design

In addition to the process equipment discussed above, the GE steam production facility also required a test section where the loss measurements will be taken. The test section is the region designed to hold the blade cascade at the designated stagger and inlet angle. To minimize the need for replacement test sections, the primary test section designed for the proposed GE steam facility includes a mechanism to adjust the blade inlet angle. To modify the stagger of the cascade, the Lexan blade mounting sections of the test section side walls (Figure 5) can be replaced with new sections specific to new stagger angles. The exit expansion rate can be controlled by modifying the tailboard angle. If the aspect ratio or scale is changed, the test section can be removed and replaced with a new section designed for the new blade geometry. Another feature of the test section is that it has been designed with one inch stainless steel walls to reduce vibrations. All interior components will be built with stainless steel to minimize the risk of introducing heterogeneous particles to the flow from iron oxidation.

The blade inlet angle and tailboard angle (Figure 5) are designed to be changed while the facility is in operation. This minimizes the costs associated with starting and stopping the facility which could take several hours. The sidewalls will be rotated by the use of servo motors, while linear actuators will move the lower inlet guide board and inlet nozzle to match the new inlet angle. The tailboard will be fixed at its upstream end to the blade cascade so that it will follow the cascade as it rotates. The tailboard angle will be adjusted separately through the use of linear actuators. The inlet guideboard is designed with a porous surface, and will be able to provide varying back pressures on the porous wall. The tailboard will be replaceable so that different designs may be used for increasing periodicity (Section 3.8).

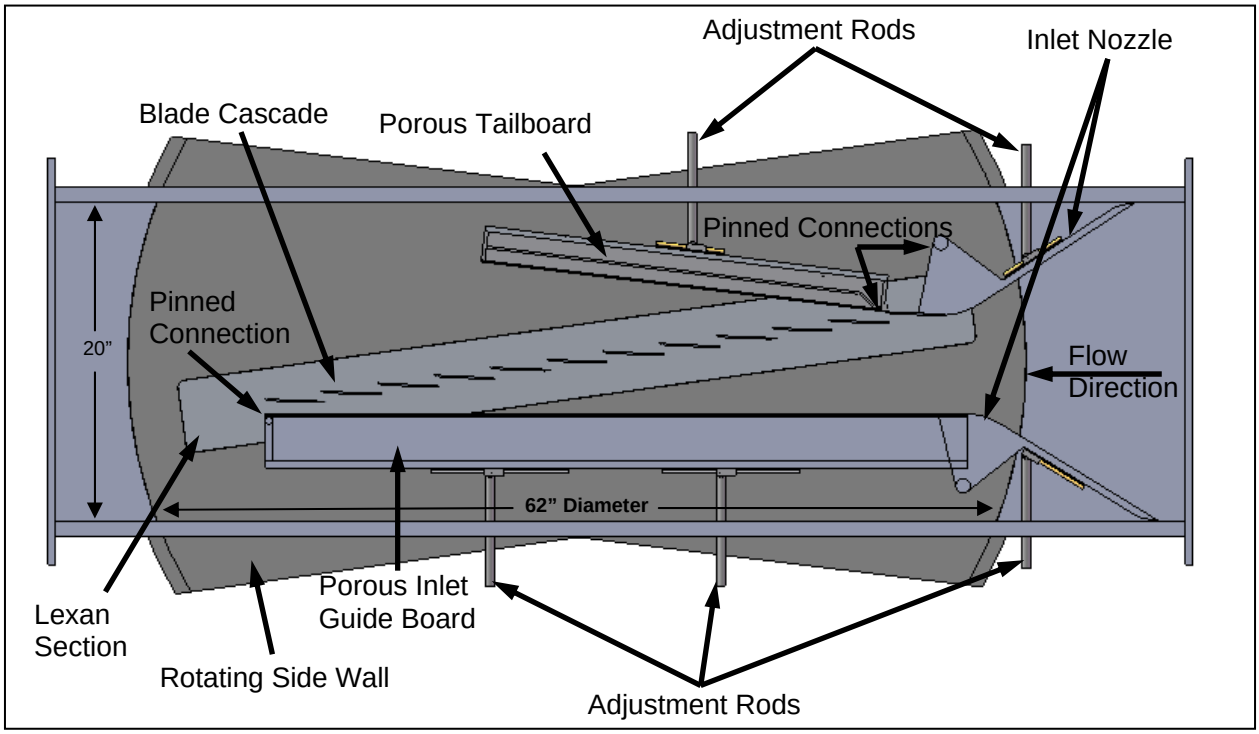

Figure 5: Test Section Layout

2.6 Facility Control

Another essential component in the design of the steam production facility is the control system, which will provide interface with, and communication between all major systems. The central controller will not provide intelligent control but will allow the operators to tune all the major equipment from one location while maintaining some automatic safety functions. A National Instruments (NI) [15] system was selected to serve as the central controller. This allows interface to occur through a standard desktop computer using LabVIEW to write and run the control program.

To control the conditions in the test section, only certain variables of each piece of equipment need to be interfaced with the NI system. Many of the pieces of equipment can be purchased with prebuilt controllers. For the steam generating equipment, a sub-

controller will control the boiler, deaerator, pumps, and make-up water to provide a pressure set point that will be determined by the required test section mass flow. The boiler control system will also provide an input of the steam exit temperature and pressure. The condenser and cooling tower system, like the steam generating system, will utilize a sub-controller to control the cooling water temperature by varying the cooling tower fan speed. The cooling water temperature will control the back pressure provided by the condenser. Inputs from this system will include the condenser pressure and exit water temperature.

The test section inlet conditions will be controlled by the boiler pressure, the throttle valve upstream of the turbine, and the turbine power extraction. The boiler pressure will control the mass flow and will therefore have a large effect on setting the Reynolds number in the test section. The turbine inlet temperature can be controlled by changing the position of the throttle valve. Changing the dynamometer back torque and therefore the turbine work extraction will allow the exit wetness to be controlled within the limits of the turbine inlet conditions. The effects of changing each of these parameters while holding the others constant are shown below in Figure 6. By adjusting these factors, the inlet wetness can be changed independently of the test section Reynolds number. Figure 7 shows the required settings for each of the three control variables to reach a given test section Reynolds number at three wetness fractions.

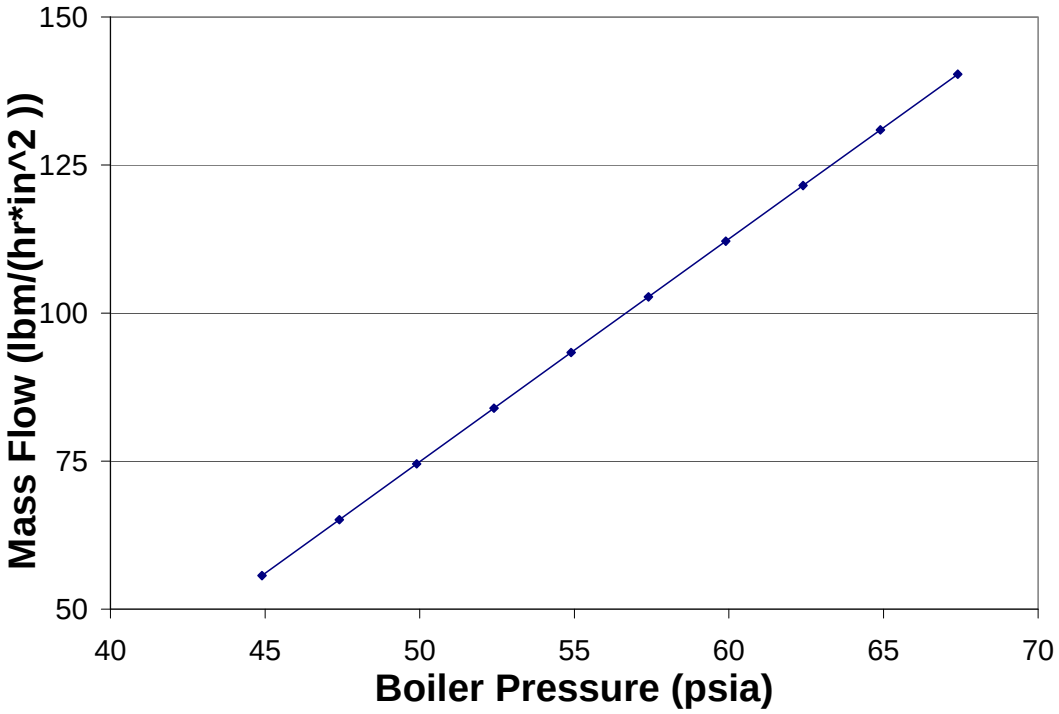

Figure 6a: Test Section Mass Flow vs. Boiler Pressure

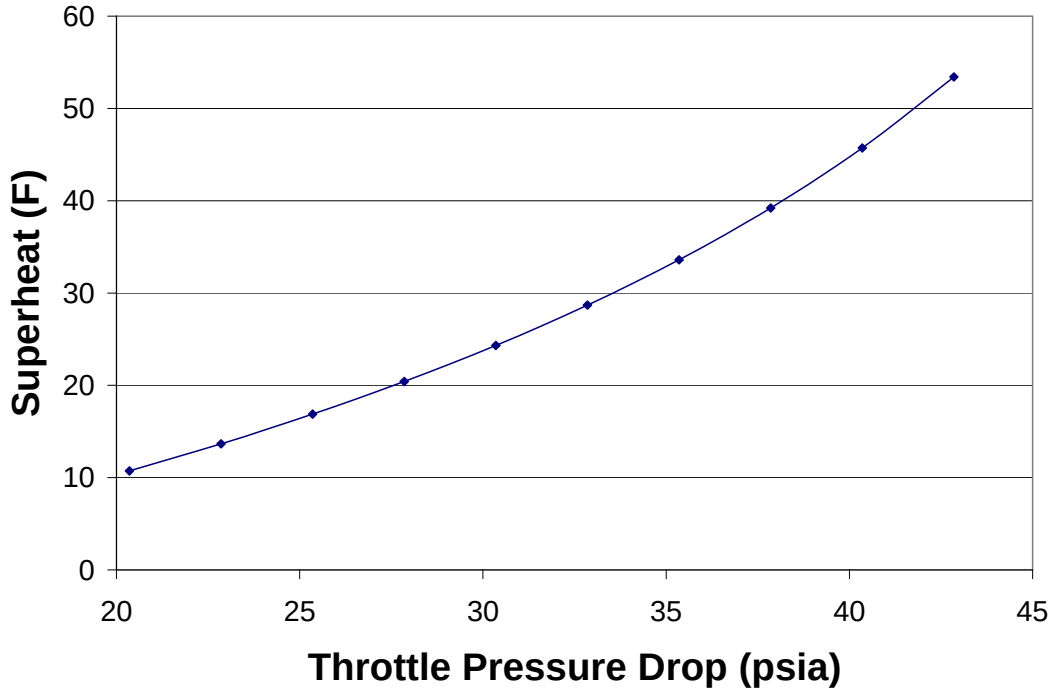

Figure 6b: Turbine Inlet Superheat vs. Throttle Pressure Drop

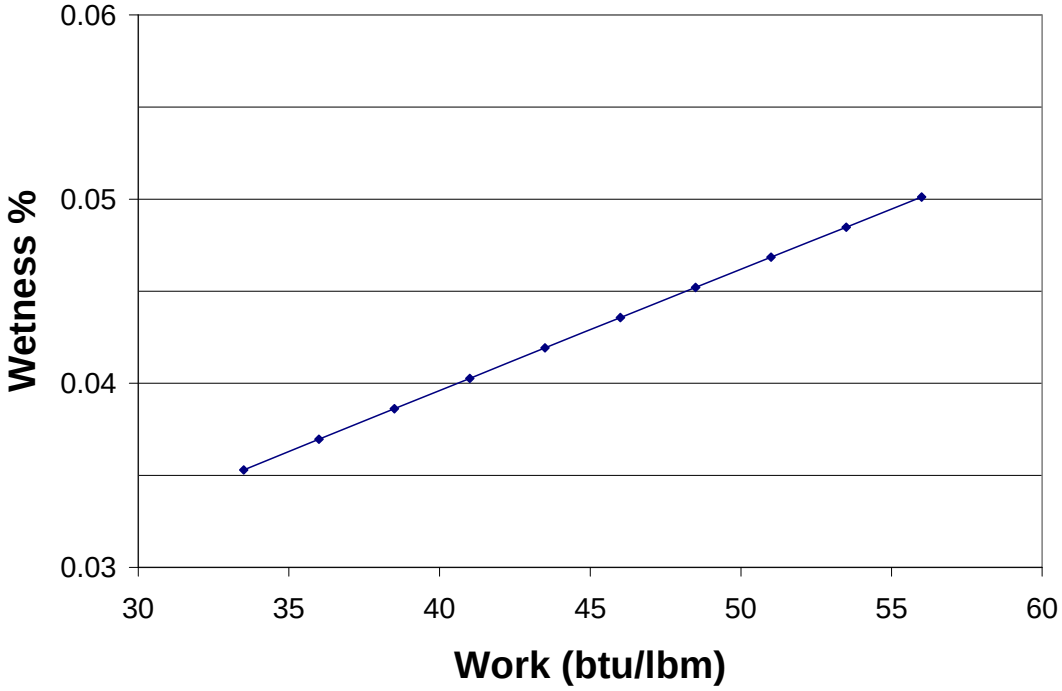

Figure 6c: Test Section Wetness vs. Turbine Work

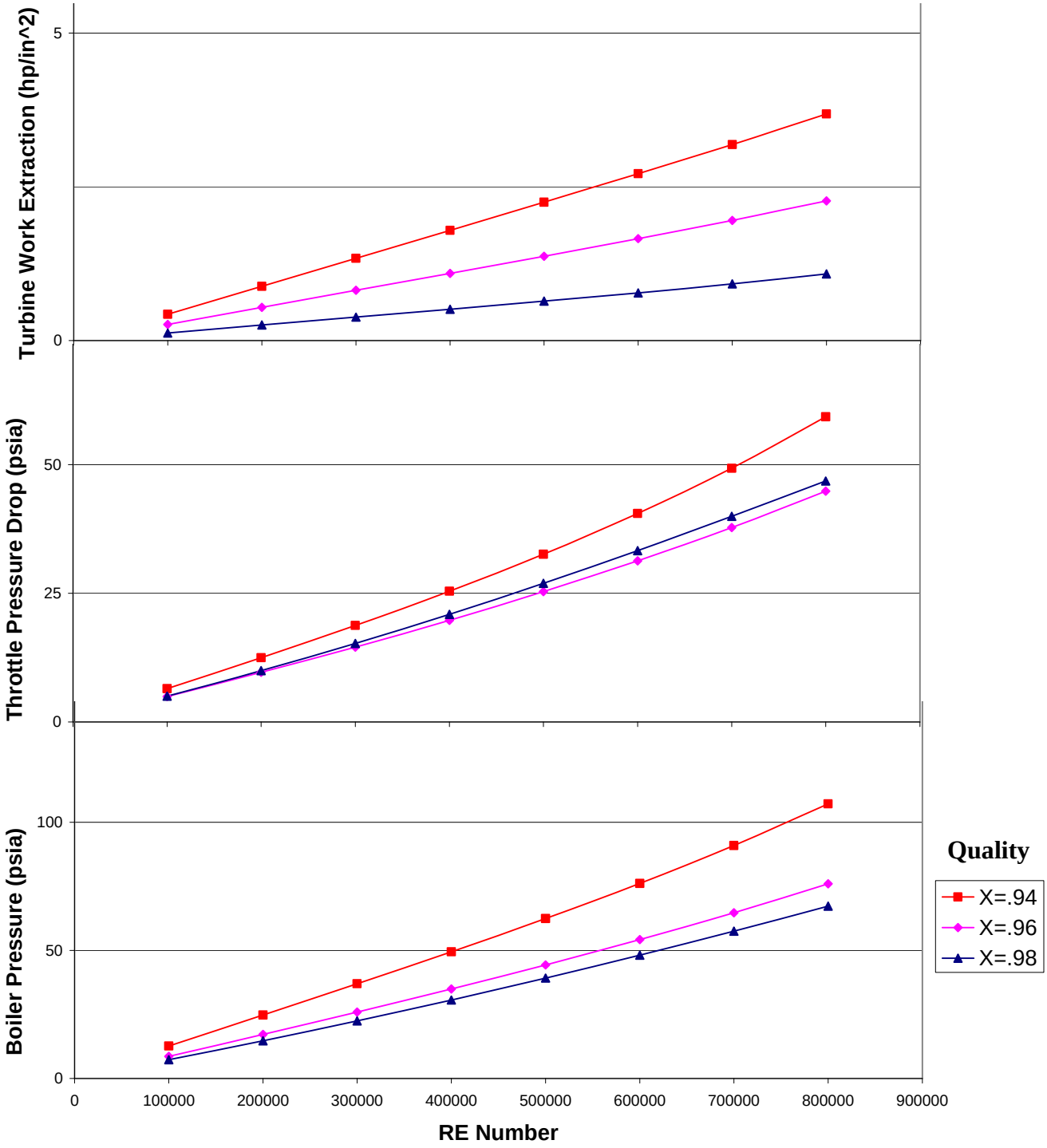

Figure 7: Control Settings for Test Section Re Number and Wetness

To control the test section geometry, the inlet angle and tailboard angle will be variable and controlled though the NI system. Two linear actuators with position feedback will control the positions of the upstream and downstream portions of the

tailboard, thus changing the angle. This will allow the expansion rates, and therefore the back pressure, to be controlled in the test section within the limits of the condenser pressure. For proper expansion, the condenser pressure should be lower than the tailboard exit pressure.

2.7 Steam Production Facility Design Summary

The steam production facility was designed for a wide range of test section conditions and with flexibility to accommodate a test section size that has yet to be determined. A quasi-Rankine cycle was selected and equipment was found for two facility variations based on the expected upper and lower bounds of the test section size. Methods for controlling the test section conditions regardless of its size were also determined. The final test section size will be determined from an additional project whose preliminary results are reported in Appendix E. Once the test section size is determined, the design of the steam production facility can be finalized quickly by selecting equipment of the appropriate size. Steam production facility cost estimates can be found in Appendix C for the larger test section size and in Appendix D for the smaller test section size.

3.0 Instrumentation

A critical problem in developing a steam cascade facility for blade performance measurements is how to instrument the test section properly to allow the blade losses to be found accurately. This problem seldom has been addressed in literature because until recently there has been limited need to determine blade losses in wet steam and those that have addressed it recently have not reported on it due to the competitive nature of the steam turbine industry. To determine the blade losses, new methods were developed that used previous instrumentation techniques in new ways and recently developed instrumentation techniques, possibly for the first time in wet steam. The second objective of this project was to design an instrumentation system for measuring blade performance. To describe the solution to this objective, literature on blade losses in wet steam, existing measurement techniques for wet steam, and non-equilibrium effects will be presented first. Then, the CFD code used to estimate the instrumentation conditions will be discussed and presented in support of the loss measurement techniques. Next, methods for measuring losses by finding the entropy of wet steam will be presented, and a modification for non-equilibrium will be shown. Finally instrumentation accuracy and periodicity problems affecting accuracy will be discussed.

3.1 Turbine Blade Losses

One of the primary sources of losses in wet steam turbines is the creation of thermal non-equilibrium between the steam and the forming water droplets. As droplets condense, the latent heat of vaporization released is initially captured in the droplets. If condensation takes place faster than the latent heat of vaporization can be transferred from the droplets to the vapor, thermal non-equilibrium between the droplets and the

vapor will occur. Equilibrium must then be restored by heat transfer across a finite temperature gradient which results in a rise in entropy of the fluid and therefore a thermodynamic loss. The process of nucleation in steam and the associated losses are described in greater detail by Guha [16].

Thermal non-equilibrium can be achieved by the rapid expansion of steam with a low degree of superheat. This rapid expansion causes the steam to move to a state within the saturation dome at a rate that exceeds the nucleation rate. This results in a meta-stable state, known as a super-cooled state, where the mixture is drier and the gaseous phase is cooler than it would be at equilibrium. Reversion from this state to equilibrium can take place by sudden and rapid nucleation where the forming droplets will rise to a temperature greater than the vapor as described above. The following transfer of heat from the droplets will raise the temperature of the vapor, which, in supersonic flows, results in a pressure rise known as a condensation shock. Condensation shocks are likely to occur at the near-tip sections of the last stage of low pressure steam turbines where expansion rates are high and the steam is near saturation.

The aerodynamic losses can also be greatly affected by the formation of water droplets and condensation shocks. In two phase steam, the compressible effects differ greatly from those in air. The position of the unity Mach line in a steam turbine blade passage can differ from the geometric throat due to condensation effects. Condensation effects will also be change the position of trailing edge shocks and bow shocks. Complex interactions between condensation shocks and sonic shocks can form, changing the aerodynamic performance. If a sonic shock forms before the supercooling of the steam is great enough to form a condensation shock, the condensation shock will be delayed or

canceled entirely. A condensation shock that occurs upstream from the sonic shock will greatly alter the location of the sonic shock. The positions of these shocks will affect the aerodynamic performance of the blade section and can result in greater aerodynamic losses. A detailed discussion on the aerodynamic effects of condensation in steam is provided by White et al. [4]. More details on nucleation, condensation shock formation, and aerodynamic interactions can be found in Appendix A.

3.2 Instrumentation for Wet Steam

The additional loss mechanisms discussed in the previous section complicate the measurement of blade losses. In traditional air cascade tests, a loss coefficient can be found based on total pressure. However, in wet steam total pressure measurements are more difficult to obtain, and an easier and more universal measurement of blade losses will be entropy generation. Because the standard measurements, temperature and pressure, are not independent in the saturation dome, additional information is required to determine the entropy. More complexity is added when attempting to determine entropy at non-equilibrium states. To overcome these difficulties, additional atypical measurements will be needed in a wet steam tunnel. Existing techniques for finding velocity, wetness, pressure, and total pressure in wet steam are described in the following section. Combinations of these measurements will be used in methods for finding entropy presented later in Section 3.5.

Many methods for finding the velocity of wet steam exist in literature. Klietz and Dorey [17] summarize a large number of these methods, including such methods as Pitot-static measurements, laser Doppler anemometry (LDA), particle image velocimetry (PIV), and hotwire anemometry. Pitot-static measurements are greatly complicated by

the complexity of the non-isentropic deceleration of wet steam. The problems and methods involved in the use of pitot-static measurements will be discussed later as they pertain to total pressure measurements.

LDA is typically used in air tunnels to determine the air velocity by measuring the velocity of small reflective particles, known as seed particles. These seed particles are introduced into the flow upstream of the test area and are chosen to be small and light enough to travel with little to no slip with the surrounding air. LDA is a successful method to find the velocity of wet steam when an adequate amount of correctly sized droplets is available for use as seed particles. LDA has the advantage of being non-intrusive to the test section flow. Details on laser Doppler methods are described by Albrecht [18]. A comparison of velocity measurements made in wet steam by LDA and total pressure probes can be found in the work of Bakhtar et al. [6, 19].

Kleitz and Dorey [17] also discuss various other techniques for measurement of velocity including PIV and hot-wire anemometry but find both to be inadequate for wet steam measurements. Hot-wire anemometry has difficulties in measuring velocity in flows carrying fluid particles and in high speed flows, both of which are present in our facility's test section. While Kleitz and Dorey wrote that PIV was unable to measure the velocity of the small droplets found in steam turbines, more recent information from Estevadeordal [20] showed that this technique is able to measure velocities for small droplets below 0.5 μm. The ability to use smaller droplets will allow better measurements to be made in the area of nucleation downstream from the cascade where some droplets may near.1 μm in diameter. The size of the water droplets needed for

LDA was larger, so PIV was selected as the method for measuring velocity in the GE steam facility.

Several methods for measuring the wetness of steam exist, but most require sampling and are extremely slow. Few methods exist to optically measure the wetness of steam. Of these methods two were investigated; phase Doppler particle analysis (PDPA) and light extinction. The light extinction method was selected because it is the only method capable of measuring wetness with water droplets below 1 μm in diameter. This method was developed beginning in the 1970s. Early measurements made using this method had large uncertainties associated with them. While these uncertainties are still relatively large, they have been greatly reduced since the light extinction methods inception.

The light extinction method was used and discussed by Moore et al. [2], Skillings [3], and Bakhtar et al. [8]. This method measures the extinction or turbidity when light passes through wet steam and correlates it to the droplet size and concentration using the Beer-Lambert law. One problem with this method is that either concentration or droplet size must be known to find the other. This can be overcome by using multiple wavelength extinction measurements. For polydispersed droplets, size groups must be created and the droplet sizes estimated. This can result in poor measurements if the droplet sizes are not accurately estimated. Very large droplets can also mask the presence of smaller droplets and make them impossible to detect; thus, very pure steam is required to ensure that no large droplets are formed by heterogeneous nucleation around foreign particles. If the droplet sizes are estimated accurately and foreign particle

minimized, a wetness fraction can be found from the size and concentration of droplet groups.

Static pressure is often one of the simplest measurements to take but requires additional attention in a wet steam tunnel. The measurement of static pressure can be impaired by the condensation of water droplets on the static taps and in the pressure tubing. The presence of droplets causes a blockage in the tube, which prevents accurate pressure readings and can harm the pressure transducers. This problem is addressed by Moore and Sieverding [4] who found periodic air purging to be the solution. Blowing the droplets clear allows accurate measurements to be taken for approximately 2 seconds between purges. Another solution found was to fill the pressure transducer lines with water, or oil and use more rugged transducers that can be in contact with liquids. This has the advantage of not introducing air to the test section but requires the use of more expensive transducers.

Total pressure measurements are complicated by the phase change of wet steam and the associated thermodynamic losses. In super-sonic flows, these problems are compounded by the presence of a standing bow shock in front of the probe tip. The interactions between the non-isentropic condensation and the bow shock are difficult to calculate. Another consideration in total pressure readings is that the wet steam reaching the probe may not be in equilibrium after passing through the standing bow shock. The losses due to condensation through the bow shock will depend on the size of the droplets in the flow. These losses will be reduced for larger droplet sizes where non-equilibrium conditions are less likely to be achieved. These factors make uncorrected total pressure readings impossible to use in loss calculations. Attempts to over come these problems

have been made by both White et al. [4] and Bakhtar et al. [7, 21]. Bakhtar has provided more detailed information on methods for calibrating total pressure probes for wet steam. These calibrations are similar to those for super-sonic air but involve wetness and droplet size as additional variables. By calibrating a total pressure probe over many wetness fractions, Mach numbers, and droplet sizes, a set of calibration curves can be made which allow the probe to be used accurately. To perform these calibrations, wetness and droplet size will also need to be found which will add to the calibration uncertainty. To reduce this uncertainty a set of calibration nozzles will need to be built which produce known Mach numbers, wetness, and droplet sizes.

3.3 Non-equilibrium Effects on Instrumentation

To use the measurement methods discussed in the previous section for accurately determining blade losses, these methods must be modified for non-equilibrium conditions, as explained in Section 3.6. Before discussing these modifications, non-equilibrium conditions must be discussed. Two main types of non-equilibrium that will affect instrumentation are thermal non-equilibrium, introduced in Section 3.1, and inertial non-equilibrium. Inertial equilibrium implies that both the phases are traveling at the same velocity. The presence of inertial equilibrium is very important for the use of optical velocity measurements such as PIV and LDA, which are only capable of measuring the speed of the liquid particles. Restoration of inertial equilibrium is an order of magnitude faster than thermal equilibrium as explained by Guha [16]. Typical inertial relaxation times for wet steam in LP turbines are 5 μs whereas the thermal relaxation times are 60 μs [13, 22]. The time required for inertial equilibrium to be restored from a disturbance can be calculated using Equation 1. This time can be shown to be negligible

for the conditions in the GE steam facility, and therefore inertial equilibrium can be assumed.

$$t_I = \frac{d^2 \rho_l (1 + 2.70Kn)}{18\mu} \quad (\mathbf{1})$$

Thermal non-equilibrium is likely to occur in condensing wet steam flows, as discussed in section 3.1. The level of thermal non-equilibrium can be measured by equation 2 where ΔT (Equation 3) is the supercooling and ΔT_{cap} (Equation 4) is the capillary supercooling of the droplet. The capillary subcooling will be very small and thus can be neglected [16]. The level of thermal non-equilibrium can there fore be measured directly as the supercooling or supersaturation ratio (Equations 3,5). Supercooling differs from superheating in that it is a measure of the temperature deviation below the saturation temperature and indicates a non-equilibrium state. When the measured vapor temperature is below the saturation temperature corresponding to the vapor pressure, the fluid is said to be supercooled. The supersaturation ratio is related to the supercooling through Equation 6. This information is covered in detail by Guha [16]. With these equations a method for measuring entropy at non-equilibrium can be found and is presented in Section 3.6.

$$T_l - T_v = \Delta T - \Delta T_{cap} \quad (\mathbf{2})$$

$$\Delta T = T_s - T_v \quad (\mathbf{3})$$

$$\Delta T_{cap} = T_s - T_l \quad (\mathbf{4})$$

$$S = p / p_s(T_v) \quad (\mathbf{5})$$

$$\ln S = \frac{h_{fg}}{RT_v T_s(p)} \Delta T \qquad (6)$$

3.4 2-D, Viscous CFD Models for Wet Steam

With the blade loss mechanisms explored, available measurement techniques found, and non-equilibrium difficulties understood, the instrumentation conditions were then estimated to design methods for calculating losses. These conditions included approximate pressure, wetness, and degree of equilibrium. CFD models were used to provide this information and are presented in the following sections to support the instrumentation design. The CFD work for this paper was done by Stephen Guillot [23] of Techsburg Inc. The CFD program used was GASP version 4 [24], which uses a RANS type solver with an additional water-vapor condensation model. Each blade was meshed with an O-mesh consisting of 221 cells in the circumferential (i-) direction and 33 cells in the radial (j-) direction. The turbulence model used was the Spalart-Almaras model. Condensation effects were modeled with the Perrell condensation model included in GASP. The condensation model was necessary to show the non-equilibrium effects in the test section. This model tracks several size classes of droplets allowing them to grow or shrink into other classes and to be created using equations for growth rate and nucleation rate. The model assumes thermal equilibrium but represents non-equilibrium condition through a calculated supersaturation ratio.

3.5 Equilibrium Entropy Measurement

As discussed in section 3.2, entropy generation will be used to measure blade losses. To determine the entropy at an equilibrium state, two methods have been developed, and will be used. The first of these methods uses a calibrated total pressure probe and calculates the entropy from the total state; the second method uses PIV to find

the velocity of the fluid particles and calculates entropy from the static state. While the use of a total pressure probe in wet steam has been reported previously, no use of PIV in wet steam has been found in literature. It is believed that the GE steam cascade facility will be the first to use PIV and the second method for finding the entropy of wet steam.

To use the entropy generation as a measure of blade losses, the entropy will need to be multiplied with the local mass flow to get an entropy generation rate (Equation 7). Thus, at each point the velocity will need to be found and a density calculated from steam table functions to find a differential mass flow. Both of these methods will be affected significantly by the degree of equilibrium achieved in the flow at the point of measurement.

$$\dot{S}'' = \dot{m}'' * s \qquad (7)$$

For both methods, the test section is assumed to be adiabatic allowing the total enthalpy to be assumed constant across the cascade. The cascade inlet total enthalpy can be calculated by determining the total enthalpy at the turbine inlet with total pressure and temperature measurements and subtracting the measured turbine work extraction (Equation 8). Both methods rely on an accurate measurement of the turbine work by the dynamometer. This measurement can initially be verified by using the static pressure, total pressure, and wetness measurements at the cascade inlet. These measurements can be used at the facility startup to calibrate the dynamometer measurements for higher accuracy.

$$h_t(T_t, P_t) - TW = h_{ts} \qquad (8)$$

For the first method, exit total pressure will be found with a calibrated traversing total pressure probe. With total enthalpy and pressure known, the entropy can be

calculated using steam property functions (Equation 9). A static enthalpy for the fluid can be calculated using exit static pressure measurements and the entropy (Equation 10), and this static enthalpy can be used with the total enthalpy to find the local fluid velocity (Equation 11).

$$s = f(p_0, h_0) \quad \textbf{(9)}$$

$$h = f(s, p) \quad \textbf{(10)}$$

$$v = \sqrt{2(h_0 - h)} \quad \textbf{(11)}$$

For the second method, a PIV system will be built that uses the water droplets present in the flow as seed particles. To use the small droplets (>.1μm) expected in the steam, advanced PIV techniques will be needed [20]. No previous examples of PIV use in wet steam have been found. This method requires that the flow be in inertial equilibrium. This can be safely assumed as discussed in Section 3.3. The total enthalpy at the test section exit will be found again using the method described above (Equation 8). A static enthalpy can be found with the total enthalpy and velocity (Equation 12), and the entropy can be calculated with static enthalpy and exit static pressure measurements using a steam property function (Equation 13).

$$h = h_0 - \frac{v^2}{2} \quad \textbf{(12)}$$

$$s = f(h, p) \quad \textbf{(13)}$$

3.6 Non-Equilibrium Loss Measurement

After establishing two methods for calculating entropy at equilibrium conditions attention was then given to the occurrence of non-equilibrium conditions in the area of measurement. CFD models made for the proposed GE steam facility show that thermal

non-equilibrium will occur in the area of measurement downstream from the cascade (Figure 8). In Figure 8, the degree of non-equilibrium is plotted as the supersaturation ratio. The areas of blue show a high degree of thermal non-equilibrium on the exit wake traverse line where measurements will be taken.

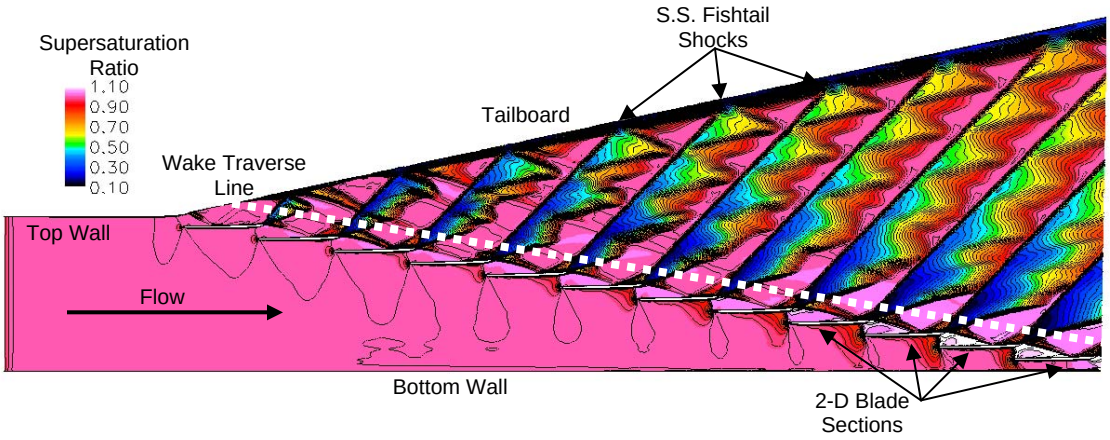

Figure 8: Non-equilibrium Condition Shown by CFD

Entropy measurements at a thermal non-equilibrium point require wetness measurements because the vapor and liquid phase are no longer at equilibrium mass fractions. Vapor and liquid temperatures can differ greatly from one another at these points; therefore vapor pressure measurements cannot be used to find the temperature of the vapor phase. However, the capillary supercooling (Equation 3) will remain very low due to the faster thermal relaxation time of water; therefore the liquid temperature can be assumed to be the saturation temperature found at the vapor pressure. Light extinction measurements will provide the droplet radius and concentration. These measurements can be made for both mono- and poly-dispersed droplets.

Only two size groups of droplets are expected: one of larger droplets formed in the steam turbine before entering the test section, and one of much smaller droplets created in the cascade. The following methods described can also be applied for larger numbers of size groups. Droplets created in the cascade are created by homogeneous nucleation and expected to be near 0.1 μm. The presence of the larger droplets created in the upstream turbine is expected to produce some amount of heterogeneous nucleation, but the expansion rate in the cascade is expected to be rapid enough to cause a significant supercooling and spontaneous nucleation. This will result in a second and much smaller size group of droplets. This was shown by White et al. [4], where condensation shocks still formed in the cascade despite the presence of existing water droplets at the cascade inlet.

With droplet sizes and concentrations, the wetness fraction contained in each size group can be found. The liquid enthalpy and entropy for each group can be found using the mechanical pressure calculated for each size and the liquid temperature (Equation 14). With this information, the vapor enthalpy can be found with the velocity produced from either method (Equation 15). The vapor entropy can be found by using the vapor pressure and enthalpy. This yields the fluid entropy and the losses when added with liquid entropy (Equation 16).

$$P_l = P_v + \frac{2\sigma}{r} \tag{14}$$

$$h_v = \frac{h_0 - \frac{v^2}{2} - y_1 h_{l1} - y_2 h_{l2}}{1 - y_1 - y_2} \tag{15}$$

$$s = (1 - y_1 - y_2)s_v + y_1 s_{l1} + y_2 s_{l2} \tag{16}$$

3.7 Loss Measurement Accuracy

The accuracy of loss measurements cannot be fully determined until the facility is in operation. While transducer errors and some estimated instrumentation errors can be determined there are additional error sources that remain unknown. The known sources of error are discussed below and their relative effect on the loss measurement evaluated.

The quantity with the largest effect on loss calculation for all methods discussed will be total enthalpy. The total enthalpy measurement will depend on the accuracy of measurements made up stream of the turbine, the turbine power extraction, and the mass flow measurement. At the turbine inlet, pressure transducers with ± 0.0025 psia accuracy will be used to measure total pressure, and resistance temperature detectors (RTDs) with ± 0.144 Rankine accuracy will be used to measure total temperature. Making these measurements upstream of the turbine allows them to be made in superheated steam where their accuracy will be much higher than in wet steam.

Power extraction at the dynamometer can be measured with a typical accuracy of ±0.23% quoted by a manufacturer. The mass flow can be measured using differential pressure measurements made with a calibrated Venturi nozzle just downstream of the condenser. This measurement is most accurate when taken downstream of the condenser, in water rather than steam. This mass flow will be the same as in the turbine and test section. The accuracy of the mass flow measurement in water was quoted by a manufacturer to be ±0.25%. Since only 7% of the total enthalpy will be extracted by the turbine at design conditions, the work extraction and mass flow measurement error will have a much lower effect on the test section enthalpy calculation than the turbine inlet measurements.

While both measurements share the same error in total enthalpy calculation each will have an independent accuracy for entropy calculation. The accuracy of method two depends on PIV velocity measurements and test section static pressure measurements. The test section pressure transducers have an approximate accuracy of ± 0.0025psi with a range of 5psig. Velocity measurements with previous PIV methods could be made with an accuracy of ±1%, but the accuracy of the new methods used for this facility is unknown. For method two the velocity measurement will likely be the largest source of error in the calculated entropy. For method one the uncertainty in total pressure calibration has not been determined and cannot be shown at this time to produce more or less accurate entropy measurements than method two.

The accuracy of entropy measurements made by both methods at non-equilibrium states will be influenced greatly by the accuracy of the wetness measurements. The wetness could be measured with an estimated uncertainty of ± 10% by Bakhtar et al. [8], making it the largest source of error in the blade loss measurements. The effect of this uncertainty on the blade loss measurements will be greatly limited as it will only be used in calculating entropy at non-equilibrium points. The error in distribution of mass between droplet size groups can be neglected because the enthalpy of liquid water has a low sensitivity to pressure change, and the differences in mechanical pressures for expected droplet sizes in the GE steam facility are small (Equation 14). The error in vapor enthalpy due to wetness error for method two can be found using Equation 17 where the error due to the distribution of mass between droplet size groups is neglected.

$$h_{v,err} = \frac{h_0 - \frac{v^2}{2} - y_{err} h_l}{1 - y_{err}} \qquad (17)$$

A 10% error in wetness has a surprisingly small effect on the entropy at a point when it is calculated using steam property functions modified for meta-stable states. With a ± 10% uncertainty in wetness, the uncertainty in entropy is well below ± 0.1% (Equation 18). These errors are again averaged with other points using mass weighting (Equation 7) which will decrease their effect on the total loss measurement of one passage.

$$s_{err} = (1 - y_{err}) * s_{v,err} + y_{err} * s_l \quad (\mathbf{18})$$

In addition to the errors from individual measurements made above, there is a possible error from assuming uniform total enthalpy in the exit flow. To use the calculated test section total enthalpy, the flow is assumed to be homenthalpic. Initial CFD results along a simulated traverse line one chord length downstream (Figure 9) show pitchwise fluctuations in total enthalpy. While it is possible for total enthalpy to be non-uniform, the level of non-uniformity reported by the CFD code was suspect and should be verified by experiment. Calculations with simulated instrumentation data from the CFD results show that pitchwise variations in total enthalpy could create significant errors in individual data points, but when data was averaged over one pitch using mass weighting (Equation 7), these errors were reduced greatly.

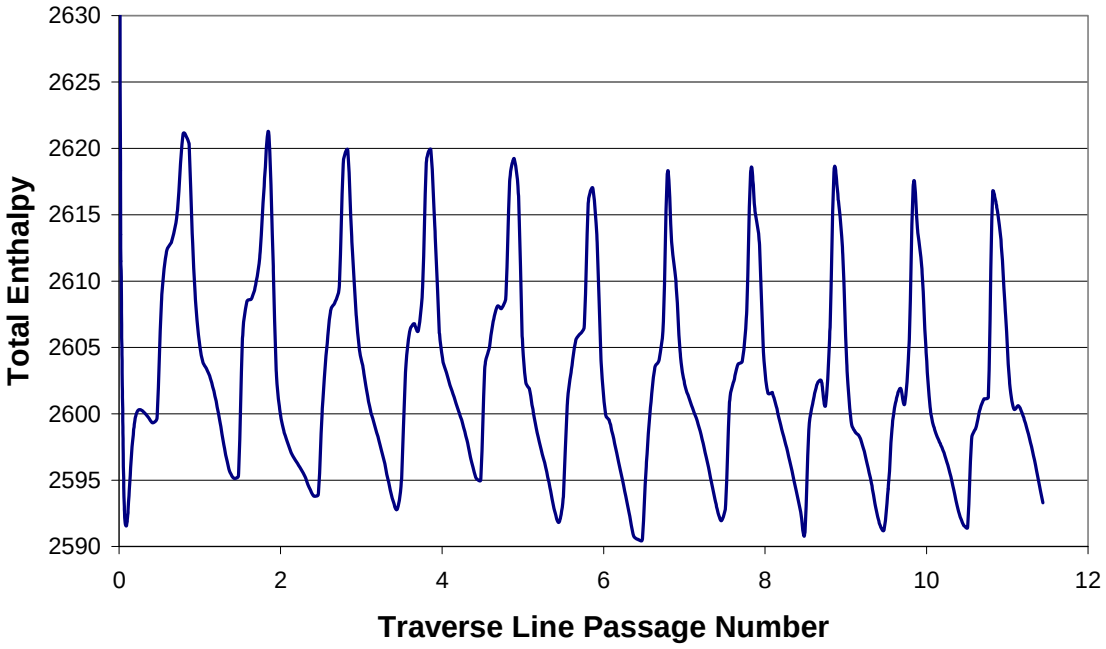

Figure 9: CFD Total Enthalpy on Simulated Traverse

3.8 Periodicity

Another consideration in the accuracy of loss measurements is the periodicity of the flow. Periodicity implies that each passage has a nearly identical distribution of properties. In an actual turbine the blades are arranged radially resulting in the flow conditions for each blade being reproduced infinitely in the tangential direction. To simulate this in a linear cascade, an area of several periodic passages must be produced. This will ensure that the blade losses measured are truly representative of the actual turbine. Early CFD work showed that periodic flow was difficult to establish, and it was thought that 12 passages were needed. Figure 10 shows early CFD results for a six passage cascade, where aperiodicity is shown by the non-uniformity of the exit Mach numbers. Even with 12 passages (Figure 11), CFD results still did not show periodic flow due to the complex interactions of reflected shocks. Figure 11 also shows the

presence of bow shocks that resulted from a small deviation in inlet flow angle, and reduce the inlet periodicity. Figure 12 shows the lack of periodicity in isentropic Mach number over the blades suction and pressure sides, where the periodic condition at a pressure ratio of 7.5 is plotted as a solid line for comparison.

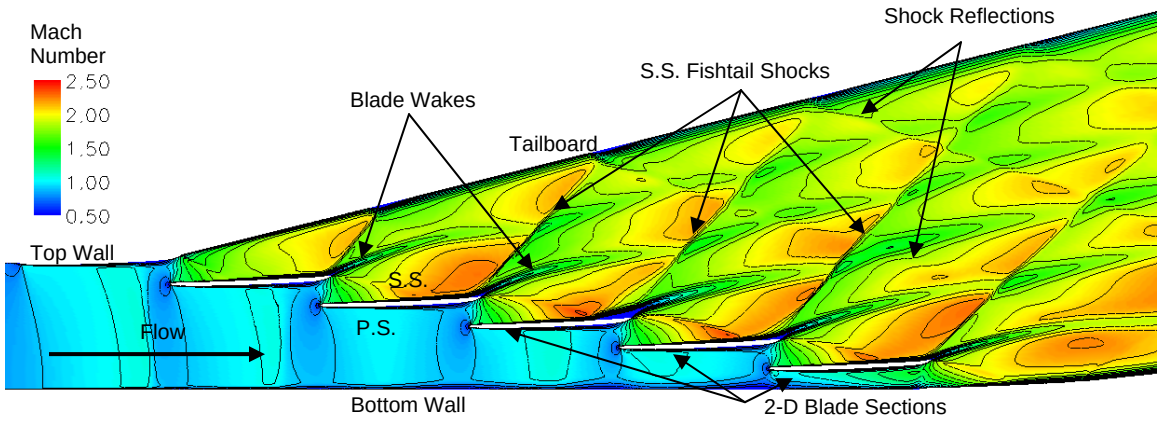

Figure 10: Early CFD Results for Mach Number Distribution

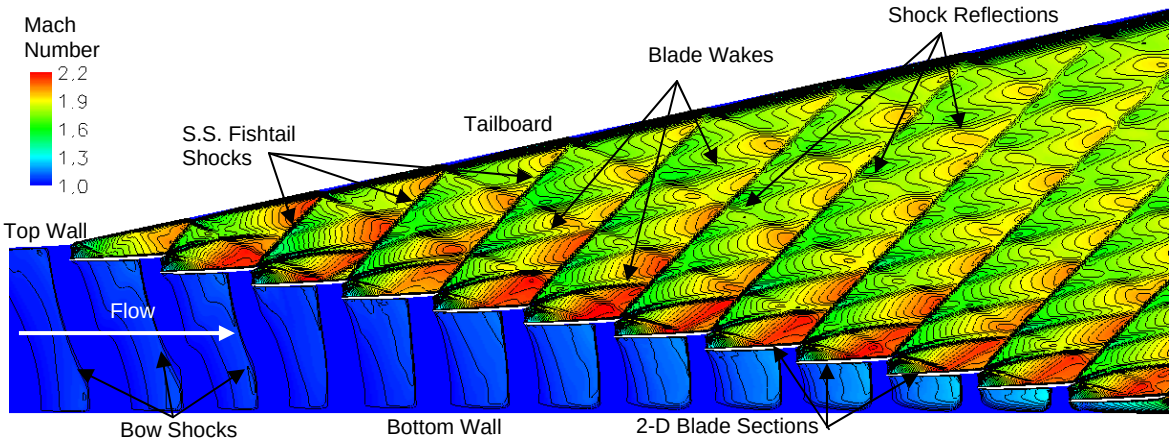

Figure 11: Large Cascade CFD Results for Mach Number Distribution

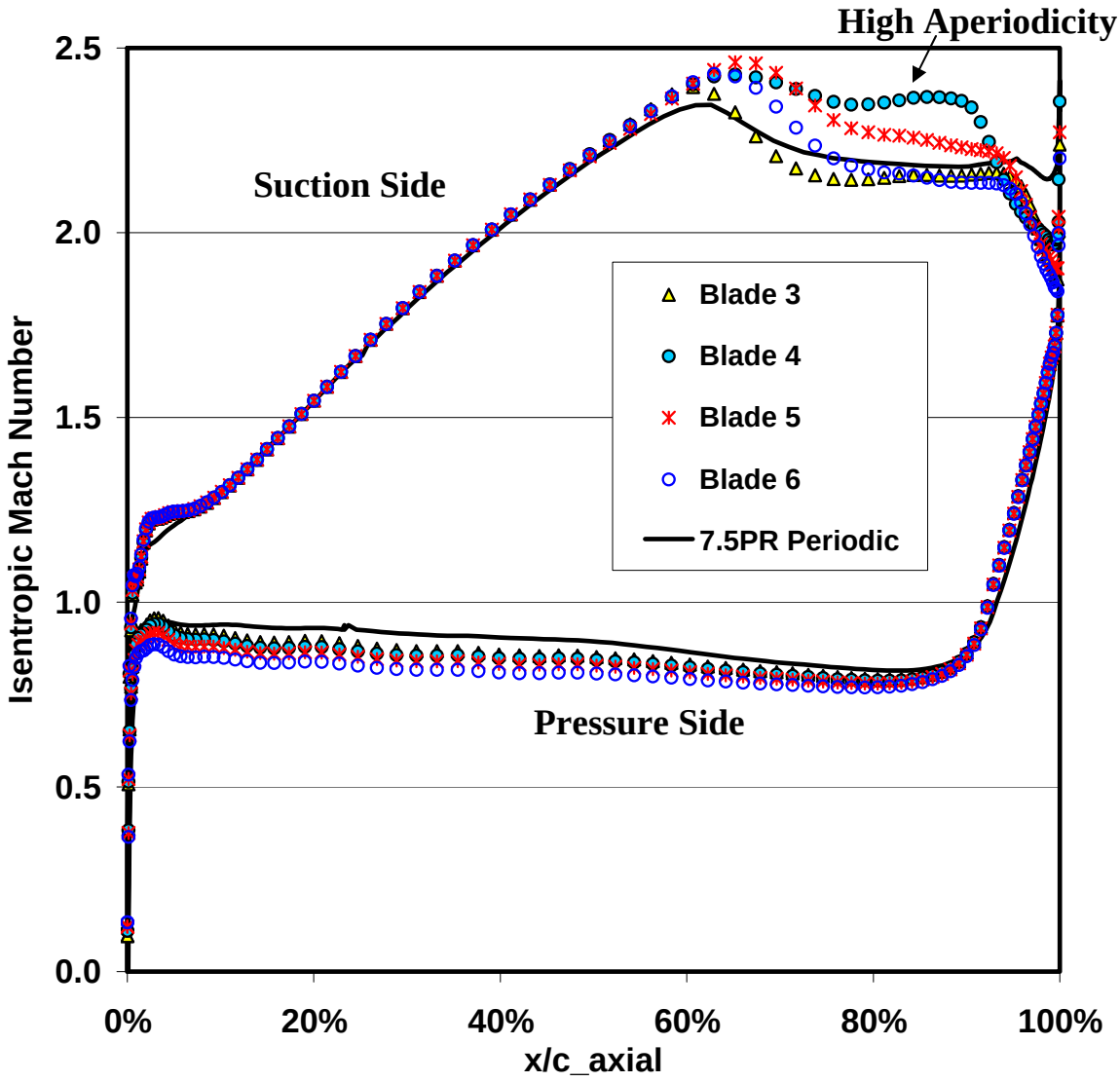

Figure 12: Non-Periodic Blade Isentropic Mach Numbers

The primary means of increasing periodicity has been to increase the number of passages, requiring a larger test section and steam production facility. Increasing the number of passages has little effect on periodicity for the GE LP turbine tip section geometry. To limit the cost of the facility, methods to improve periodicity and limit the number of passages were needed. It was decided that a second project, discussed in Section 2.2, was needed. The work for this project was done in an air cascade to explore

potential methods for improving periodicity while limiting the number of passages. In addition to testing these methods tests would also be conducted to determine if the aspect ratio could be reduced. The results of this project are beyond the scope of this thesis, but preliminary results from the air cascade tests are reported in Appendix E.

The first method to check the periodicity in the proposed GE steam facility will be to use shadowgraphs. Shadowgraphs allow density gradients, and therefore shocks and expansion waves, to be seen in the upstream and downstream flow field. The test section will be built with Lexan windows (Figure 5) designed for both the PIV and shadowgraph equipment, providing access to both upstream and downstream conditions. By adjusting the cascade inlet angle, the exit tailboard angle, and using other advanced shock wave reflection canceling techniques, periodicity in cascade should be achieved and shown by shadowgraphs. In addition to the visualizations of the shock and expansion waves, sidewall static pressure taps will be used to check the inlet and exit flow fields. Blade surface pressure taps will also serve as a means for checking the inlet and exit periodicity. A final check on the periodicity of the exit flow will be the data taken with either method to determine the blade losses.

3.9 Instrumentation Summary

The instrumentation system was designed to be capable of accurately determining blade losses in a wet steam cascade. To accomplish this a measurement of blade losses was first determined to be the entropy generation, since the more traditional method of total pressure drop was not well suited for wet steam. Available measurements for wet steam were identified and two methods were formed using combinations of these measurements to find entropy. To improve the accuracy of these methods a modification

was made to allow measurements to be taken in non-equilibrium conditions. Finally the accuracy of these methods was discussed by showing the relative importance of individual measurements and considering periodicity issues, which are expected to create the largest uncertainty in loss measurement.

4.0 Conclusion

From the work presented in this paper the proposed GE steam facility design was completed and will be used to construct the facility when it is approved. To complete the design for the GE steam cascade facility two major objectives were identified; 1) design a steam production facility, and 2) design a system for measuring the blade performance.

The first objective was completed by designing a new steam production facility using only limited information from previous facilities. Literature on these facilities was first discussed. The test sections conditions were then determined for a blade model scale (blade span / chord length) of 0.5. The aspect ratio and passage number were left as variables in the equipment requirement calculations and shown to only affect the required mass flow rate. Flexibility for the yet to be determined test section size was incorporated by designing two steam production facility size variations for the upper and lower most expected test section size. The final test section will be determined by a second project that is beyond the scope of this thesis. Preliminary results from this project are reported on in Appendix E.. A quasi-Rankine cycle was selected to provide the steam flow. This cycle was modeled in a Matlab code, and the results were used to select equipment. Equipment options were found for both a large 12 passage, 1.5 aspect ratio test section and a smaller 8 passage, 0.75 aspect ratio test section. A means to control the test section conditions with this equipment was then found, and specific equipment settings were

shown for a range of test section wetness' and Reynolds numbers. The required equipment, vendors, and costs are shown in Appendix C and Appendix D for the large and small test section sizes respectively. While the steam production facility is likely very similar to existing GE competitor facilities, the proprietary nature of such facilities made the design work necessary for the new steam production facility.

To complete the second objective of this project a new blade loss measurement system was designed. Blade loss mechanisms, various existing measurement techniques, and non-equilibrium effects found in literature were first discussed. Entropy rise was determined to be the best measure of blade losses, and two methods were proposed for determining entropy. The first method used a total pressure probe and was modified from previous methods presented in literature. The second method proposed the use of advanced PIV techniques to find the velocity of the steam and, with static pressure measurements, provide the steam entropy. This method has not been found in any existing literature and may also be the first use of PIV for high speed wet steam. A modification to allow both of these methods to take more accurate measurements at non-equilibrium conditions was then proposed. This method used the light extinction method to find wetness, which has been used in previous literature, but this is possibly the first use to find the entropy of a non-equilibrium state. The accuracy of these methods was then discussed and the relative importance of individual measurements to the overall accuracy was shown. Finally the largest accuracy risk for loss measurements was shown to be the difficulty in establishing periodicity in this facility. Periodicity problems were discussed with CFD results and the need for a second project to determine the required test section size was presented (Appendix E).

The work presented in this paper establishes that the construction of a steam cascade facility for testing blade performance is feasible and that performance data can be obtained for the GE LP turbine tip section geometry. A large amount of additional engineering work will be needed before construction can begin, but the concepts have been proven in this paper. Also, an additional project to determine methods for increasing periodicity in the cascade was undertaken as a result of the findings of this first project. Early results from this additional project along with the work of this paper shows that the GE steam facility could be built at the smaller proposed size with an estimated cost of one million dollars.

Appendix A: Condensation Shocks

Condensation shocks develop in rapidly condensing steam or water vapor flows. These phenomena occur when steam crosses into the saturation dome faster than the equilibrium processes can take place, resulting in fully gaseous steam at a temperature and pressure that correspond to a mixture of liquid and gaseous phases. Condensation shocks cause a small increase in pressure, density, and entropy, making them similar to weak sonic shock.

A.1 Nucleation Process

To understand the effect of condensation shocks on steam turbines, the fundamental process of nucleation must first be understood. This process is explained in simple nozzles by Guha [16]. Two types of nucleation can occur: heterogeneous and homogeneous. Heterogeneous nucleation occurs where there are existing solid particles that the steam then condenses onto. This process of nucleation occurs at a rate many orders of magnitude faster than homogenous nucleation, and so the formation of a condensation shock is unlikely. In the absence of heterogeneous particles, steam must condense by the process of homogeneous nucleation. This process requires a finite amount of time to occur, known as the relaxation time. When there is insufficient time for homogeneous nucleation to occur, a non-equilibrium or meta-stable state is temporarily formed.

Non-equilibrium can be achieved in many different ways, but the two primary modes of non-equilibrium that affect condensation in steam turbines are inertial and thermal non-equilibrium. Inertial equilibrium relates to the speed of water droplets versus the speed of the steam. As water droplets condense, they are initially able to move at a

different speed. This difference in speed can be due to drag forces and depends largely on the size of the droplets. For inertial equilibrium to be restored there is an associated relaxation time known as the inertial relaxation time. Thermal non-equilibrium results from a difference in the liquid and vapor phase temperatures. The associated relaxation time is known as the thermal relaxation time. Inertial relaxation occurs at least an order of magnitude faster than thermal relaxation, and so its effects are usually neglected.

Another type of equilibrium effect that must be accounted for results from the surface tension forces on a droplet, and is known as mechanical equilibrium. This equilibrium is achieved nearly instantly and thus does not have a relaxation time associated with the condensation process. However, its effects are important when considering the thermodynamic state of a liquid droplet. The net result of achieving mechanical equilibrium is that the pressure forces within a droplet are much higher than in the gaseous phase. The conditions for mechanical equilibrium are shown below in Equation A.1. All other types of non-equilibrium that can occur have relaxation times many orders of magnitude faster than thermal non-equilibrium and so are not considered in the nucleation process.

$$p_l - p = 2\sigma / r^* \qquad \textbf{(A.1)}$$

In steam turbine blades, thermal non-equilibrium is often reached when the steam is quickly expanded to super-sonic speeds. This expansion results in the gaseous state crossing into the saturation dome at a rate which exceeds the thermal relaxation time for homogeneous nucleation. Impurities in power plant steam turbines are in low enough concentrations that the steam must condense by homogeneous nucleation. As the steam enters the saturation dome, it remains dry and behaves as a gas, allowing it to reach lower

temperatures than are possible by equilibrium conditions. This effect can be seen below in Figure A.1, where steam at pressure P continues to cool to past the equilibrium temperature Te to a temperature Tv within the saturation dome.

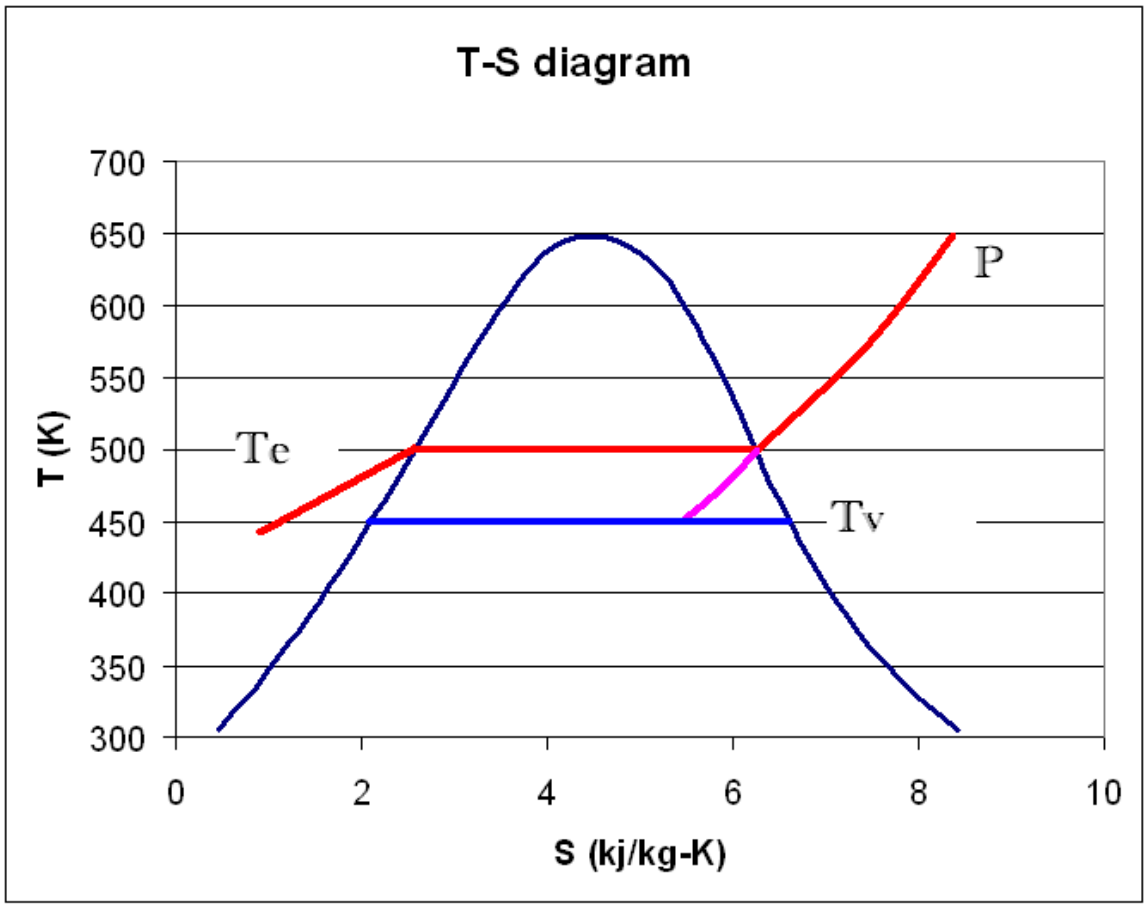

Figure A.1: T-S Diagram for Non-Equilibrium

The degree of thermal non-equilibrium is measured as super-cooling defined below in Equation A.2. It can also be measured by the saturation pressure ratio where the saturation pressure at T_v and the actual pressure are used as shown in Equation A.3. The two can be related by Equation A.4.

$$\Delta T = T_s - T_v \quad \textbf{(A.2)}$$

$$S = p / p_s(T_v) \quad \textbf{(A.3)}$$

$$\ln S = \left(\frac{h_{fg}}{R \cdot T_v \cdot T_s(p)} \right) (T_s - T_v) \quad \textbf{(A.4)}$$

The degree of super-cooling will define the state of the steam and can be used to predict its behavior. When steam reaches a critical degree of super-cooling, which can be as high as 30-40°C, it will undergo a sudden and rapid nucleation process where a very large number (10^{14} to 10^{17} nuclei per kg steam) of very small nuclei (diameter < 1nm) are created, as explained by Guha [16]. This point is known as the Wilson point and corresponds to an equilibrium wetness of 3-4%. The resulting rapid release of latent heat from the condensed nuclei will result in a temperature rise in the steam. In super-sonic flows, the temperature rise will result in a decrease in velocity and a rise in pressure. This rise in pressure is the condensation shock.

Often steam will enter the last stage of a LP turbine with previously formed droplets. These droplets will act as seed particles and result in partly heterogeneous condensation during the expansion. With seed particles available for nucleation, the degree of super-cooling obtained will be greatly reduced. The amount of heterogeneous condensation that takes place will be proportional to the available surface area of the seed particles.

The nucleation process will result in a finite temperature difference between the droplets and the steam. As steam condenses out onto existing droplets, it will give up the latent heat of vaporization to the forming droplet. This heat will then have to be released back to the steam to restore thermal equilibrium, and this heat transfer across a

temperature gradient will result in an increase in entropy. This loss is referred to as the thermodynamic loss and is the largest loss associated with wet steam flows.

The degree of super-cooling achieved by the steam as it reaches a meta-stable state can be found by using the Gibbs free energy equations. For a given temperature and pressure in the saturation dome, a critical droplet radius will exist called the Kelvin-Helmholtz radius. This radius corresponds to the highest free energy, known as the free energy barrier. Droplets formed below this radius will evaporate, while droplets formed above this radius will grow. The critical radius is defined below in Equation A.5.

$$r^* = \frac{2\sigma T_s}{\rho_l h_{fg} \Delta T} \qquad \textbf{(A.5)}$$

This equation shows that for any degree of super-cooling, one size of droplet will form. This size is in unstable equilibrium with the surrounding super-cooled steam. From this equation, it can be seen that for any droplet radius in steam there is an associated super-cooling. A droplet radius of 0.5μm corresponds to a super-cooling of less than 1°C. It can also be seen that a high degree of super-cooling results in very small droplets (<20nm).

Classical thermodynamics can not account for the formation of droplets above the critical radius, as the initial droplet growth must involve an increase in free energy. The use of chemical kinetics allows for random interactions of water molecules to form larger droplets through collisions. A chemical rate equation was created to explain the formation of droplets larger than the critical radium. This equation is defined below in Equation A.6 where J_{cl} is the nucleation rate.

$$J_{cl} = q_c \frac{\rho_v^2}{\rho_l} \sqrt{\frac{2\sigma}{\pi m_w^3}} \exp\left(-\frac{\Delta G^*}{kT_v}\right) \qquad \textbf{(A.6)}$$

As the degree of super-cooling becomes greater (and therefore so does the degree of non-equilibrium), the critical radius becomes smaller as does the activation energy for nucleation. With lower activation energy, the nucleation rate increases. The limit where the rate of nucleation has become so great that it exceeds the rate of cooling or expansion occurs near an equilibrium wetness of 4%. Steam cannot remain in a meta-stable, super-cooled state beyond this point, referred to as the previously mentioned Wilson point.

Now that the nucleation process is understood, the formation of a condensation shock can be viewed from a different perspective. In combustion and compressible flow theories, a shock wave can be defined by the Rankine-Hugoniot shock jump relations. For combustion problems, a detonation wave can be defined as a jump from the Hugoniot of the reactant mixture to the Hugoniot of the products mixture at higher pressure.

A condensation shock can be viewed in the same way as a detonation wave because the process of condensation can be seen as a release of chemically stored energy. When the steam is in a thermal non-equilibrium state and has not condensed, its temperature has dropped below its equilibrium value. The formation of liquid droplets results in the release of the latent heat of vaporization to the steam flow. This allows for the steam at one state to jump to a Hugoniot line of higher energy. It can be shown that this results in an increase in density and pressure.

A.2 Aerodynamic Interactions

While Guha explains the process of nucleation in simple nozzles, more complex interactions must be investigated in the case of turbine blade cascades. To understand the formation of the sonic shock waves and the expansion process in steam turbine blades, one must first understand the geometry of an LP turbine blade.

Gostelow [25] provides a good explanation of the unique problems associated with last stage LP turbine blades. In order to obtain greater power from LP steam turbines it, has been necessary to increase the exit area. This has lead to inlet relative velocities in the tip section that must approach or exceed the local speed of sound. These high velocities will result in the formation of a bow shock. The exit Mach number of the blade row at the tip section can be as high as Mach 1.8, resulting in exit oblique shocks. With both inlet and exit sonic shock waves established, the interaction of the condensation shock becomes increasingly complex.

A discussion of the complex interactions between sonic shock waves and nucleating flows can be found in Skillings [3] and White [4]. Skillings noted in his research that the complex geometry of blade passages results in different rates of expansion on the suction and pressure sides of the passage. The fastest expansion rate occurs near the suction surface, resulting in a greater degree of super-cooling and earlier nucleation. Skillings's experiments showed the formation of a distinct condensation shock under certain conditions that resulted from the differing expansion rates.

White [4] presented a more detailed analysis of the interactions between condensation shocks and sonic shocks while performing experiments to validate condensing flow models. White found that the formation of the condensation shock can be further complicated by the impingement of the pressure-side trailing-edge shock of the adjacent blade on the suction surface. This sonic shock can have different effects under varying inlet wetness and Mach number.

White found that when the inlet steam was superheated, a zone of super-cooled steam was still created in the blade passage, but no condensation shock formed at any

inlet Mach number. This was explained by the fact that the sonic shock from the adjacent pressure-side trailing edge effectively canceled the super-cooling before a condensation shock could form. This cancelation can be explained by the fact that sonic shocks increase both the pressure and temperature of the steam and dry it.

Under low inlet superheat conditions, a distinct condensation shock formed upstream of the sonic shock (Figure A.2). By varying the inlet Mach number, a situation could be made where the sonic and condensation shocks crossed. This resulted in two separated condensation shocks occurring for suction and pressure sides. Under wet inlet conditions with droplets of diameter 0.5μm, White observed that the condensation shock was delayed as compared with dry saturated inlet conditions, which is explained by the fact that the existing droplets allowed for some amount of heterogeneous condensation to take place.

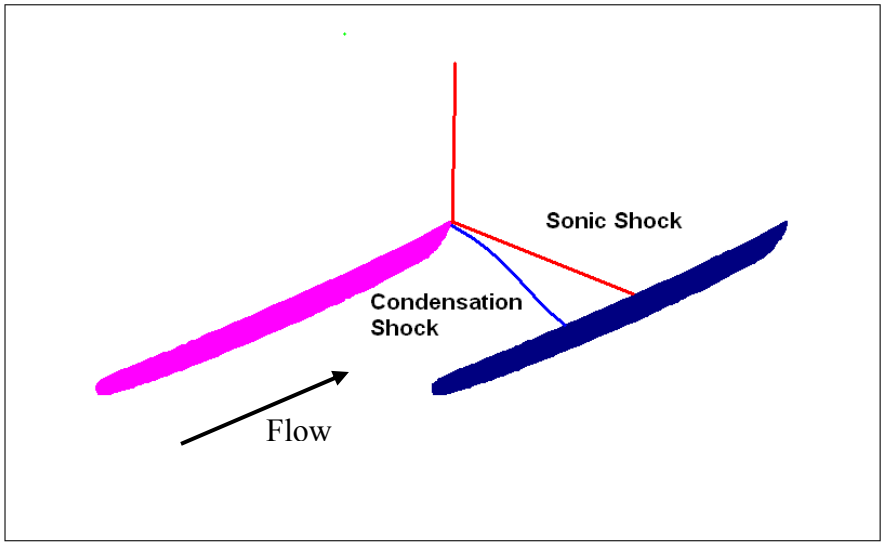

Figure A.2: Blade Sonic and Condensation Shocks

Appendix B: Cycle Selection

Two main cycles were considered to produce the required conditions in the test section. The first idea was to use a method similar to the Rankine cycle used in power plants. This cycle will be referred to as the condensing cycle. The second idea was to eliminate the need for condensing and reheating the steam by repressurizing the saturated steam exiting the cascade using a compressor in a cycle similar to the Brayton cycle. This cycle will be referred to as the compressor cycle. Other modifications to these cycles were also considered as possible solutions.

B.1 Condensing Cycle

For each cycle a basic model was constructed and calculated in a Matlab program. For the condensing cycle 6 key states were found between the different components of the cycle (Figure B.2).

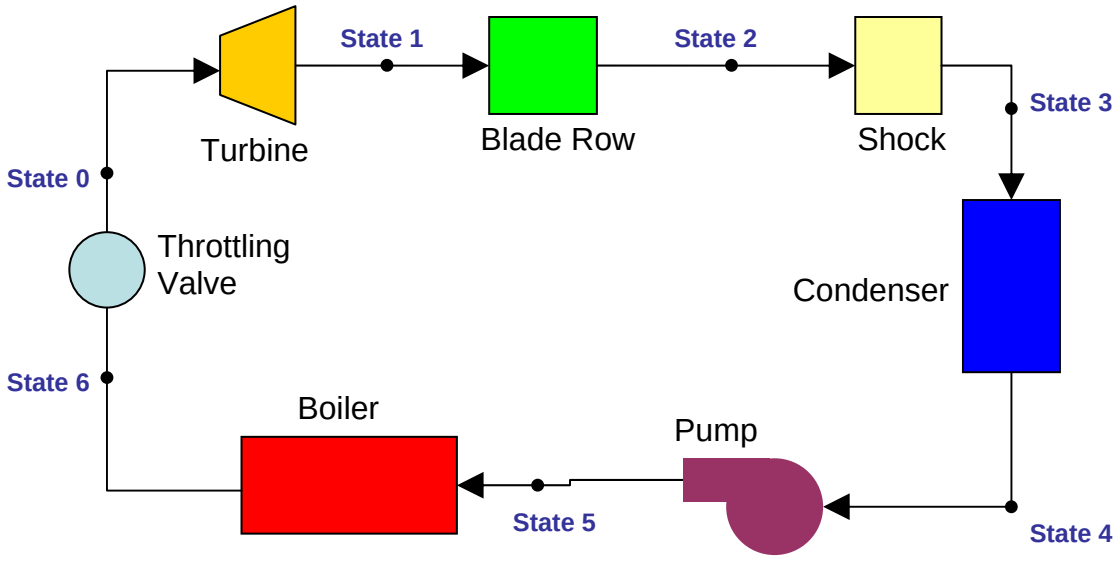

Figure B.1: Condensing Cycle Diagram

Each of the key states was determined by finding the thermodynamic properties and the velocity. The velocity is often found by assuming an area for the flow rate found for the test section. The methods used to find these values are discussed below for each state in order beginning from the test section inlet.

States 1 and 2 represent the locations immediately upstream and downstream of the cascade respectively. With the combination of the test section conditions provided by GE, an assumption of adiabatic flow across the blade row and a selection of the geometric scale, the thermodynamic properties of the flow at States 1 and 2 can be determined for a given Reynolds number. In addition to setting the geometric scale, an aspect ratio and the number of blades in the test section were provided as a user defined inputs to the MATLAB model. Together, these data determined the cross sectional area of the test section. This, combined with given Mach number and properties of fluid, determined the mass flow of the system

State 0 occurs at the inlet to the turbine located upstream of the test section. The turbine is designed to condition the flow entering the test section to be as representative of the flow within the steam turbine as possible. By controlling the power extraction of the turbine, the quality of the steam entering the test section is controlled. This will allow water droplets to form within the turbine rotor in a manner similar to that which would occur in the actual machine. To guarantee that the water droplets are formed within the turbine and are not present prior to entering the turbine, it is required that steam at State 0 be superheated by 25 degrees. The calculation of the remainder of the state variables at State 0 can be achieved by working backwards from State 1 using an assumed isentropic turbine efficiency.

State 6 was added in as the exit state from the boilers. Since the boilers will produce saturated dry steam it will be necessary to superheat the steam using a throttling valve. This state is fixed by using the required inlet pressure and temperature for the turbine and then working back to a dry saturated state with the same total enthalpy. It is assumed that the throttling valve will be highly non-isentropic, but will be adiabatic.

State 3 is located down stream from the shock wave. This state was determined using the separated flow model along with the conditions at state 2. The separated flow modeled used the conservation of mass, momentum, and energy to find the final state.

State 4 for the condensing cycle was defined to be after the condenser and before the pump. This state was defined to be at the same pressure as state 3, and at zero quality. Assuming the area to remains unchanged and using conservation of mass, a velocity could be determined. Using these quantities, the state could be fully defined.

State 5 is between the pump and the boiler. After leaving the condenser the condensate will need to be pressurized by a pump to the pressure required at state 6, assuming pressure losses in the boiler are negligible. Using the pressure at state 6, an assumed pump efficiency, and an assumed area the rest of the properties can be found for state 5 using the steam property functions and the conservation of mass equation.

Finally, the power input for the boiler can be determined using the mass flow rate and the change in enthalpy between States 5 and 6.

B.2 Compressor Cycle

States 6 to 4 for the compressor cycle are identical to those of the condensing cycle (Figure B.2). In the condensing cycle the total pressure drop across the test section and subsequent shock are overcome using a pump. This requires that the steam first be

condensed and then later run through a boiler. As a result of this process, a substantial amount of heat is lost to the atmosphere via heat transfer in the condenser. To avoid this energy loss, the compressor cycle uses a gas compressor to over come the pressure drop of the test section and shock. By avoiding the energy loss associated with the condenser, the require energy input into the system is substantially lower for the compressor cycle than the condenser cycle, as will be described in the Summary. The drawback, however, is that compressing gaseous steam is substantially less practical than pumping liquid water, and an industrial steam compressor was never found.

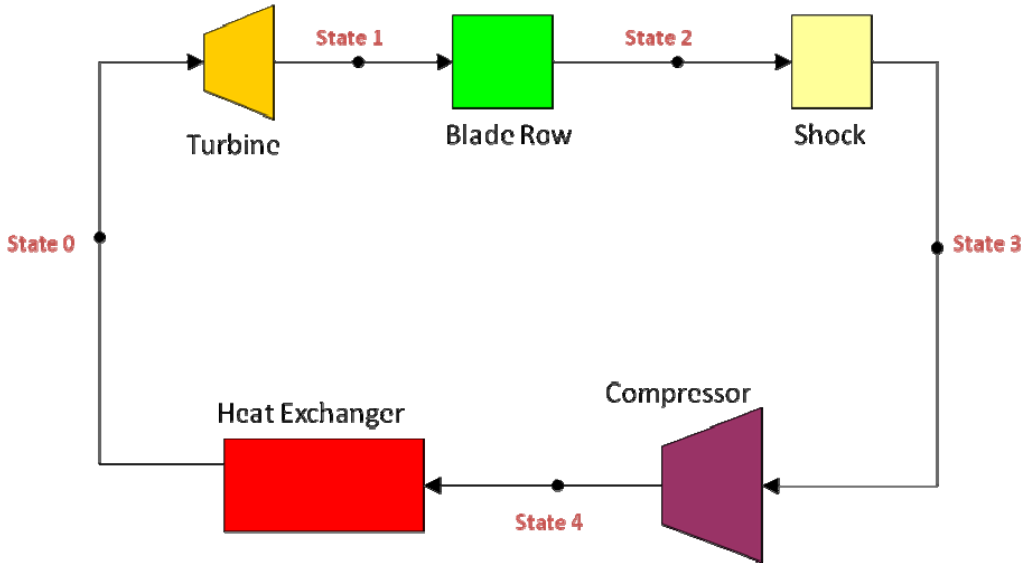

Figure B.2: Compressor Cycle Diagram

State 4 for the compressor cycle is defined to be after the compressor and before a heat exchanger. The heat exchanger will be needed to remove heat created by the compressor. Using an assumed isentropic compressor efficiency, an assumed area, and the pressure at state 4 to be the pressure at state 0, the rest of the thermodynamic properties can be found using the steam property functions and the conservation of mass

equation. The total heat removal was found by assuming the rest of the cycle to be adiabatic. A throttling valve will not be required as the degree of superheat at inlet to the turbine can be controlled by the heat exchanger.

B.3 Alternative Configurations

In order to increase the efficiency of both cycles several alternatives were considered. For the condensing cycle a heat pump was considered for transferring heat from the condenser to the boiler but this was found to have only marginal gains and the needed equipment was unavailable. It was also considered that the condenser could be removed from the cycle and the steam exhausted directly to atmosphere after the test section. This was quickly ruled out because the total pressure at the test section exit was found to be below atmospheric pressure. This meant no amount of static pressure recovering could raise the pressure high enough to exhaust to atmosphere.

For the compressor cycle a steam ejector pump was considered to replace the compressor which was unavailable from industrial manufacturers. To provide the motive steam for the ejector pump a high pressure condensing cycle would be required. This removed the advantage of compressing the steam compared to condensing it. Also the pressure of the motive steam was found to be too high to handle safely in common industrial type boilers.

B.4 Summary of Results

Using the two models developed in MATLAB a thermodynamic analysis was performed on both potential solutions. From this analysis the theoretical energy usage was found for each cycle and compared. The compressor cycle was found to require approximately 1/8th of the energy the condensing cycle would require. This is due to the

large amount of heat rejected from the condensing cycle in order to condense the steam. Using the models developed, an approximate size of the equipment was found. The much greater power requirement of the boiler is offset by the fact that it will use fuel rather than electricity, making both solutions feasible to operate.

The condensing cycle was selected in the end due to the availability of all major pieces of equipment needed. The compressor cycle offered a unique and more energy efficient option, but steam compressors are not used in many industrial applications. Since no manufacturers of steam compressors were found the solution had to be ruled out in favor of the more conventional condensing cycle.

Appendix C: Cost for 12 Passage, 1.5 Aspect Ratio

The cost for the facility was calculated for the worst case scenario of an aspect ratio of 1.5, 12 passages, and a scale .5. For this size test section roughly 30,000lbm/hr of steam is required. The flow rate of steam is the main factor controlling the cost of the facility. Cost factors such as building space, additional engineering, and installation labor costs were not included. All costs contain an estimate of tax and inflation, and some costs include a scaling factor because the equipment specifications and cost quote were not made for the full mass flow rate. The total cost for this facility was found to be 1.56 million dollars, and is shown below in table C.1 with the costs broken down.

Steam Generating Equipment	456103
Condenser	48750
Cooling Tower	61800
Piping and welding	64871
Test Section	150000
Turbine	467500
Dynamometer	220000
Instrumentation and Controls	249055
Total	1718079

Table C.1: Cost List

The steam generating equipment prices included all equipment necessary for the boilers to take in condensate and produce dry saturated steam. The cost for the steam generating equipment is broken down into its individual equipment in table C.2. The equipment list includes three Cleaver-Brooks FLX1200 boilers, stacks, and upgraded burners for additional turndown ratio. With the Profire II burners the turndown ratio for each boiler was increased to 10:1. This will allow a total system turndown ratio of 30:1 which will allow the tunnel to idle with the lowest possible fuel consumption. A chemical feed system and deaerator were included for oxygen removal from the system.

A surge tank is required to store make-up water for the system, and insure the boilers will not run dry during a blow down or if a large amount of condensate is lost through a leak. A blow down separator and heat recovery system were added to recover heat and condensate from regular boiler blow downs. The final piece of equipment included in the steam generating equipment cost was the water treatment system. The water treatment for the make up water will consist of a water softener to remove heavy minerals from tap water before it is added to the surge tank.

Steam Generating Equipment					
Qty	Equipment Model	Cost	Scale	Total	Notes
3	Cleaver-Brooks FLX200-1200-15ST	80500	1.2	289800	Scaled for Inflation
3	Cleaver-Brooks CBS II stacks	5659	1.2	20371	Scaled for Inflation
3	Profire II burner	4099	1.2	14756	Scaled for Inflation
1	Cleaver-Brooks 100-P-V-10 chemical feed system	5380	1.2	6456	Scaled for Inflation
1	Industrial Steam packaged tray type deaeration system	43351	1.5	65027	Scaled for inflation, size
1	Industrial Steam packaged surge tank system	26988	1.5	40482	Scaled for inflation, size
1	Industrial Steam heat recovery system	7058	1.5	10587	Scaled for inflation, size
1	Industrial Steam blowdown separator	3020	1.2	3624	Scaled for Inflation
1	Water King RF-240-TA skid mounted water softener	5000	1	5000	Estimated
Total				456103	

Table C.2: Steam Generating Equipment Costs

A condenser was sized originally for a mass flow of 15,000lbm/hr of low pressure steam with and high temperature (140F) cooling water. This condenser had an effective cooling area of approximately 2100 sq.ft. This cooling area is sufficient to handle a much larger flow rate of steam with cooling water provided by a cooling tower at 85-

100F. To account for the increased cost of handling twice the steam flow rate the cost was increased by a factor of 50%. This is consistent with other quotes that were obtained for various condensers at lower flow rates. The cooling tower was sized for approximately 5500hp of heat rejection. The 12 passage configuration requires roughly double this heat rejection. Based on the costs of smaller cooling towers that were also specified and quoted the price of the cooling tower is expected to be roughly 50% greater than the original quote.

The cost for the major stainless steel piping was estimated for the full mass flow but with a two boiler system in mind. The addition of third boiler is not expected to greatly affect the original price, but this price was calculated using the smallest possible facility footprint and any increase in this footprint will result in a higher price. For this reason the piping cost includes a 50% increase in cost to account for a different facility site with longer piping runs. The piping was estimated using a cost per foot of pipe at various diameters quoted in December of 2007. The test section price was estimated by the Techsburg shop facility. This price includes machining and materials, where all pieces are to be constructed of stainless steel.

The turbine quoted for this mass flow was a two stage turbine produced by Dresser-Rand turbines. This turbine is capable of handling the large mass flows with low pressures. The two stage turbine is not ideal for this scenario, and has a greatly diminished isentropic efficiency of roughly 50%. The decreased efficiency will result in the turbine producing a greater amount of work output than desired, up to 900hp. The increased work load will be within the capabilities of the dynamometer quoted from Kahn industries. This dynamometer is capable of handling up to 2000hp of power

dissipation, and will handle 1000hp at approximately 4000rpm and over. This dynamometer is well suited to any speed, and power that the turbine is expected to operate at. The cost of both the turbine and dynamometer are scaled by 10% to accommodate any price inflation and possible additional taxes.

The instrumentation package quoted for the system includes the costs of all instrumentation required to operate the tunnel and acquire data for blade performance (Table C.3). The instrumentation cost will not vary based on the mass flow and were only scaled by an additional 10% to accommodate taxes and inflation. The instrumentation package includes remote industrial type sensors quoted by Omega. These sensors include high accuracy RTD temperature sensors and pressure transducers needed to fix the operating conditions of the boilers, turbine, and condenser. System mass flow will be found with a flow nozzle placed in the boiler feed water. The test section conditions will be found with a high accuracy 100 channel Pressure System Incorporated system capable of direct contact with wet steam.

Two traverse systems with seven hole Aeroprobe total pressure probes were included for simultaneous continuous inlet and exit traverses. A calibration section will be needed in for calibrating these probes in wet steam. The cost of this section has not been determined and is not included in the price. A National Instruments [15] Compaq data acquisition system was included with LabVIEW software to acquire data and provide control over major facility systems.

Instrumentation and Controls					
Qty	Equipment Model	Cost	Scale	Total	Notes
3	RTD Omega P-M-1/10-1/4-6-O-P-3 Turbine Inlet Temp	90	1.1	297	Scaled for Inflation
2	RTD Omega P-M-1/3-1/8-9-1/2-G-3 Condenser Temp	104	1.1	229	Scaled for Inflation
6	P trans Omega PX305-015AI Turbine and Condenser pressure	300	1.1	1980	Scaled for Inflation
1	P trans Omega PX305-015AI Condenser Level	300	1.1	330	Scaled for Inflation
1	Flow Nozzle	1000	1.1	1100	Scaled for Inflation
2	Traverse	2000	1.1	4400	Scaled for Inflation
2	7 hole Probe Aero Probe CPS7-6159-500	3500	1.1	7700	Scaled for Inflation
100	PSI system 4400 transducers	1350	1.1	148500	Scaled for Inflation
1	NI compact DAQ	4337	1.1	4771	Scaled for Inflation
1	NI LabVIEW	2499	1.1	2749	Scaled for Inflation
1	Particle Imagining Velocimetry (PIV) System	70000	1.1	77000	Scaled for Inflation
Total				249055	

Table C.3: Instrumentation Costs

The final cost for this system is provided as a best estimate, and will require refinement when a site is located for construction. Quotes for equipment will have expired before construction and so costs including an inflation allowance only serve as an estimate for equipment cost at time of construction.

Appendix D: Cost for 8 Passage, .75 Aspect Ratio

The cost estimate contained in appendix C can be greatly reduced if fewer passages are required and the aspect ratio is reduced. The results found from the air cascade tests indicate that periodicity is not improved beyond 8 passages, and that the aspect ratio can be reduced to .75 while maintaining a sufficient area of two dimensional flow.

The steam generating equipment and turbine cost can be significantly reduced compared to the costs shown in appendix C (Table D.1). The mass flow required for this smaller sized test section is approximately 10,000lbm/hr. This mass flow is one third of the mass flow required for the 12 passage, 1.5 aspect ratio case presented in appendix C. Due to this lower mass flow rate the costs of the condenser, cooling tower, and piping were scaled to approximately 75% of there original quotes that were made for a mass flow of 15,000lbm/hr. The test section cost and instrumentation costs will be unaffected by the reduced mass flow.

Steam Generating Equipment	199106
Condenser	24375
Cooling Tower	30900
Piping and welding	32435
Test Section	150000
Turbine	143000
Dynamometer	220000
Instrumentation and Controls	249055
Total	1048872

Table D.1: Costs

The mass flow will be just within the capabilities of one Cleaver-Brooks FLX1200 boiler. All other steam generating equipment required will be reduced in size but it is estimated the cost will only be reduced by a factor of 25% (Table D.2). The

turbine quoted for the scenario in appendix C is a very large custom built model that will be unnecessary for a reduced mass flow. A Dresser-Rand 703LP single stage condensing turbine was quoted as possible solution to the appendix C scenario but was incapable of handling the large mass flows at low pressures. This turbine is well suited for 10,000lbm/hr of low pressure steam and has significantly reduced cost. Since this turbine will operate at a wide range of speeds it is recommended that the Kahn dynamometer quoted in appendix C be mated to this turbine as well.

Steam Generating Equipment					
Qty	Equipment Model	Cost	Scale	Total	Notes
1	Cleaver-Brooks Model FLX1200-15ST	80500	1.2	96600	Scaled for Inflation
1	Cleaver-Brooks Model CBS II stacks	5658.5	1.2	6790.2	Scaled for Inflation
1	Profire II burner	4099	1.2	4918.8	Scaled for Inflation
1	Cleaver-Brooks Model 100-P-V-10 chemical feed system	5380	1	5380	
1	Industrial Steam packaged tray type deaeration system	43351	1	43351	
1	Industrial Steam packaged surge tank system	26988	1	26988	
1	Industrial Steam heat recovery system	7058	1	7058	
1	Industrial Steam blowdown separator	3020	1	3020	
1	Water King Model RF-240-TA skid mounted water softener	5000	1	5000	
Total				199106	

Table D.2: Steam Generating Equipment Costs

The total cost of reducing the test section to 8 passages and an aspect ratio of .75 is expected to be approximately 1 million dollars. This will present a roughly 50% savings compared with a 12 passage, aspect ratio 1.5 facility. It should be noted that with this reduced facility size will come reduced facility versatility

Appendix E: Preliminary Results of Air Cascade Project

In designing the GE steam cascade facility, initial CFD calculations showed that achieving periodicity would be difficult for a cascade of these tip sections (Section 3.8), due to the numerous shock wave reflections impinging on the cascade (Figure E.1). CFD models run with both steam and air as the working fluid showed the same periodicity problems. These problems are common to blade geometries of last stage tip sections of large diameter LP steam turbines. The larger diameter leads to high inlet speeds, high stagger angles and small turning angles (Figure E.2). These geometric conditions make it certain that reflected shockwaves will intersect the cascade. With shock waves intersecting regularly on the cascade periodic exit conditions will be difficult to achieve.

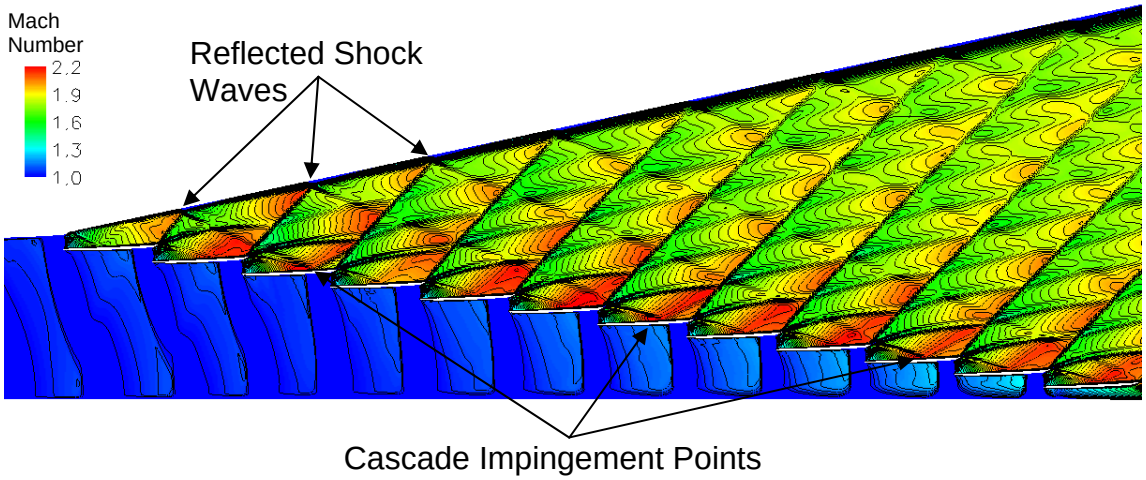

Figure E.1: Aperiodic CFD Results for a Solid Tailboard

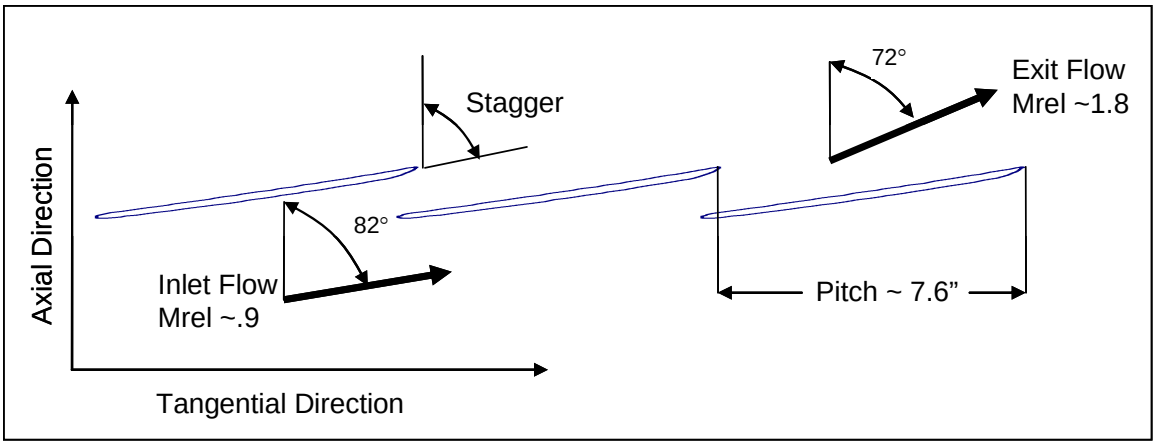

Figure E.2: Blade Geometry and Flow Conditions

Periodic conditions imply that each passage has a nearly identical distribution of properties. In an actual turbine the blades are arranged radially resulting in the flow conditions for each blade being reproduced infinitely in the tangential direction. To simulate this in a linear cascade an area of several periodic passages must be produced. This will ensure that the blade losses measured are truly representative of the actual turbine. To study the effects of condensation on this geometry in the GE steam facility the periodicity problems had to be resolved first. Without periodic conditions there would be no way to know if the blade loss measurements taken in the steam facility would accurately represent the losses in an actual LP turbine.

The need to establish periodic flow in the cascade was the main factor in determining the overall size of the steam facility. The simplest method to establish periodic flow is to increase the number of passages. As the number of passages increases the flow conditions will approach those of an infinite cascade. This is a costly method however and will increase the amount of steam flow required and the overall capitol and operating costs of the GE steam facility. Various solutions to reduce the cascade size and

establish periodic flow were first tested with CFD models, but the complexity of these solutions made the CFD results questionable. For this reason it was decided that experimental results would be needed. The periodicity issues were determined to be purely aerodynamic effects that were not affected by steam condensation. Because of this, it was decided that tests could be conducted in an air cascade using an existing wind tunnel facility. To conduct these tests the GE air cascade was built.

To establish the minimum cascade size required for the GE steam facility the GE air cascade was used to find the minimum aspect ratio required and to test the effectiveness of various tailboard configurations on the flow periodicity. The tailboard configurations tested were a solid tailboard, a porous tailboard, a shaped tailboard, and no tailboard. The preliminary results for these tests are presented in the following paper. The effectiveness of these tailboard configurations was measured by shock angles shown in shadow graphs, and blade surface pressure taps for the preliminary results only. These preliminary results showed that the aspect ratio could be reduced to 0.75 and that periodic flow could be established with 8 passages using a shaped tail board.

E.1.0 Literature Review

The available literature on air or steam cascades with similar geometry to that of the GE facility is limited in part because few LP turbine cascades exist. While the problems in achieving periodic flow are common to LP turbine cascades they are often not addressed in many experiments. However, methods for establishing periodicity in blade cascades with different geometries was found for both air and steam cascades. These methods were to use no tailboard, a solid tailboard, a porous tailboard, a slotted tailboard, and a contoured tailboard.

Gostelow [25] provides an introduction to dealing with the associated shock waves of super sonic and transonic cascades. In this book methods for dealing with the trailing edge shocks of last stage LP turbine rotors are discussed. The use of a free expansion with no tailboard is the primary method discussed and is the most common. The free expansion of a supersonic jet into a body of stagnant air creates a shear layer where shock waves will be reflected as expansion waves. These reflected expansion waves will intersect the cascade and result in poor periodicity.

Another common method to control the cascade exit discusses by Gostelow is the use of a solid tailboard. This allows the expansion rate of the exit flow to be controlled and the pressure ratio across the cascade to be controlled. The solid tailboard will provide a straight streamline at the cascade upper boundary. This will not follow the actual stream lines in an infinite cascade, and will lower the periodicity. Also as shock waves intersect with the solid tailboard they will be reflected back into the cascade as shock waves resulting in lower periodicity as well.

Porous walls with adjustable porosity were suggested by Gostelow as a means to cancel impinging shock waves. Gostelow showed that in order to cancel an impinging shock wave a mix of a free shear layer and a solid flat plate must be used. The portion of the shock that intersects the holes in the tailboard will reflect off a shear layer as an expansion wave. The remaining part of the shock wave will reflect of the solid portion of the tailboard as a shock wave. By adjusting the porosity it is possible to have the reflected expansion and shock waves cancel at some distance away from the tailboard thereby leading to a more periodic exit flow.

White et al [4], used porous tailboards in their research with turbine blade sections in wet steam. The blade sections used had greater turning angle and much lower inlet and exit mach numbers than the GE facility blade sections, but were also transonic. The research provided results for the use of unbounded exit flow, solid tail boards, and perforated tail boards. It was found that perforated tailboards provided the least disruption and best periodicity. It was noted that for best results adjustable porosity of the tailboards was desirable.

Another use for porous walls is found in work by Parvizinia et al. 2004 [10]. This research was conducted at a steam cascade tunnel owned by Siemens Power generation and sited in Mulheim, Germany. Little information is available on the design of the facility but information is provided on the design of the test section. Instead of a typical converging-diverging nozzle the diverging section is replaced by a zone of porous side walls where mass flow can be bled off. This has the effect of expanding the steam and increasing its velocity. Another important result of this technique is that inlet shocks are removed through the porous walls without disturbing the inlet flow. This technique requires higher mass flows as a large portion of the steam is bled off before the test section.

The Siemens facility used LP turbine blade geometry very similar to the geometry being tested in the GE steam facility. The research presented for this facility discussed both the inlet and exit periodicity achieved but did not discuss the methods used for controlling the exit flow and periodicity. It can be seen in this paper that the Siemens facility cascade dumped into a very large volume. It was hypothesized that the addition of a large volume with a controlled back pressure could possibly yield another method by

which to control the shock reflections created at the cascade exit. This method was tested with CFD models but its effectiveness could not be determined because the solutions were unsteady.

An additional example of the use of porous tailboards in a linear cascade of turbine blades is reported on by Paciorri [26]. In this paper Paciorri discussed the design of a numerical model of porous walls for use in CFD codes. By improving the existing CFD codes, porous walls can be optimized without the need for additional experimental time. Paciorri conducted an experiment using a cascade of gas turbine blades with geometries very different to those of the GE steam facility. A porous wall was used for the tailboard surface. This tailboard had an initial void ration (area open to area closed) of 50%. This yielded a high degree of reflected expansion waves, indicating that the void ratio needed to be reduced. Through the use of the numerical model developed the porous wall void ratio was optimized to 14.3% and implemented in the cascade.

The next approach to achieving periodicity in the GE steam facility found was to use a tailboard with a slotted wall. Rona [27, 28] describes the use of slotted walls and their optimization, and builds further on the work of Paciorri. The slotted walls described by Rona consist of a plate with channels cut in the pitchwise direction. Rona used multiple slot widths and void ratios and discovered that a void ratio of 14.3% was optimal with fewer wider slots producing better periodicity than a greater number of narrow slots. The periodicity was compared with an index of error resulting from a lack of periodicity. The results presented in these works seemed to show that optimizing the void ratio was very important but none of the results seemed to indicate that tailboards with slotted walls were more effective than tailboards with porous walls.

Another approach to improving periodicity in a linear cascade is to shape the passage walls around the blades to mimic the flow field of an infinite cascade. This approach is found in the work of Vicharelli and Eaton [29]. This paper described a method referred to as the inverse-design procedure to shape the walls around a single turbine blade to create a two passage cascade that will accurately represent the flow in an infinite cascade. In a normal cascade tailboards and addition blades are used to establish an area of periodic flow in the center two to three passages. Using the inverse design procedure the walls around a single passage are designed to reproduce the flow found in a CFD calculation for an infinite cascade. These boundaries are far different from those found in the actual turbo machine but can reproduce the actual flow characteristics. This method will be investigated as a means to achieve periodicity in the GE air cascade. A problem with this method is that the exit angle and pressure ratio are difficult to adjust without the need to design and construct new walls.

E.2.0 Facility Setup

The GE air cascade was constructed to be placed into an existing variable Reynolds number, transonic cascade wind tunnel facility. This facility operates as a "pull-through" wind tunnel that uses an air ejector pump to pull ambient air through the cascade section. The motive air for the ejector pump is provided by two 3,500 gallon air tanks pressurized to 217psia. The air provided by the tanks is sufficient to operate the tunnel for greater than 8 seconds at steady state conditions. The release of this air through the ejector pump is controlled by a pneumatic control valve (Figure E.3).

The cascade Reynolds number can be controlled by varying the inlet total pressure from below 1 psia up to nearly atmospheric pressure. This is accomplished

through the use of an inlet butterfly valve that can be manually adjusted before a test. The suction created by the ejector pump at the cascade exit can be controlled by another manually adjusted butterfly valve located just upstream of the ejector suction side. By adjusting these valves the cascade Reynolds number can be controlled independently the total pressure.

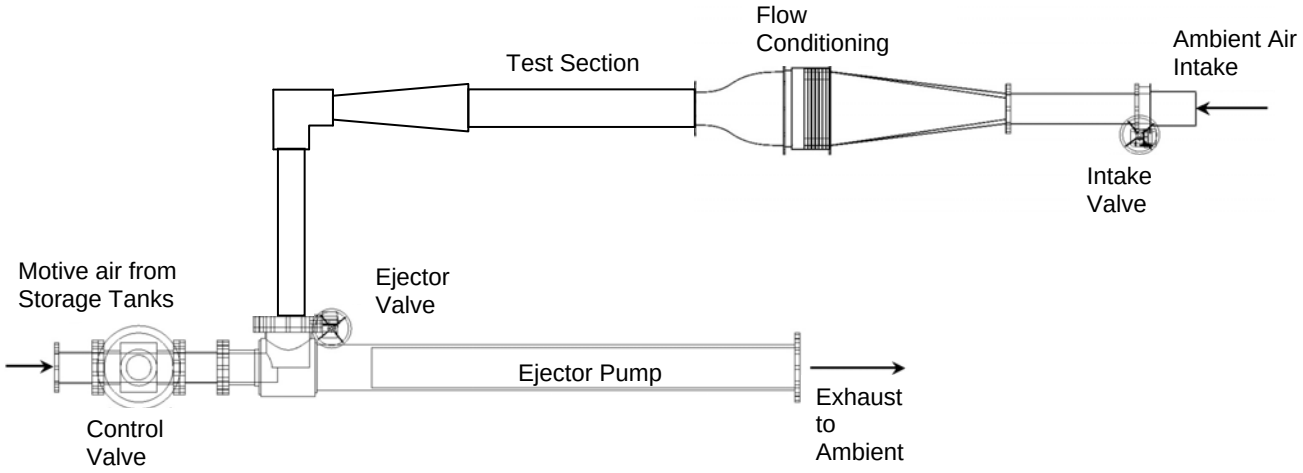

Figure E.3: Schematic of the Cascade Test Facility

E.2.1 Test Section Design

The test section consisted of eight passages of GE LP turbine tip section profiles. Eight passages were chosen because initial CFD results showed that periodicity was not significantly improved above eight passages. Also the facility mass flow limitations limited the test section size. The scale of the blades was chosen to be 0.5. This scale was chosen because it was the smallest scale that resulted in a design within the limits of machining. Instrumenting the blades with mid span pressure taps also limited the thickness and scale.

The blade profiles had a chord length of approximately four inches and a span of three inches giving an aspect ratio of 0.75. This aspect ratio was low when compared with similar experiments that were published. Initial experiments were carried out with a five inch span with and aspect ratio of 1.25 which is a more commonly accepted value. Flow visualization on the 5 inch span blades showed an effected end wall zone of less than .5" on each side attributed to the large acceleration in the blade passage. Higher pressure ratios were desired than could be achieved with the five inch span and so the span was reduced to three inches. Results from the flow visualization test are discussed in section E.3.1.

The test section was constructed of one inch thick aluminum walls. Each sidewall had an approximately 48x20 inch mounting hole for a Lexan window designed to mount the blades at the desired stagger and inlet angle (Figure E.4). The windows were designed to be replaced if different geometries were tested. These windows also allowed shadow graphs to be taken. The Lexan was susceptible to scratches that interfered with shadowgraphs but it was determined to be the best material available for mounting the blades and taking shadowgraphs. To get traverse data during a test one Lexan window could be replaced with an aluminum window with slots cut for the traverses.

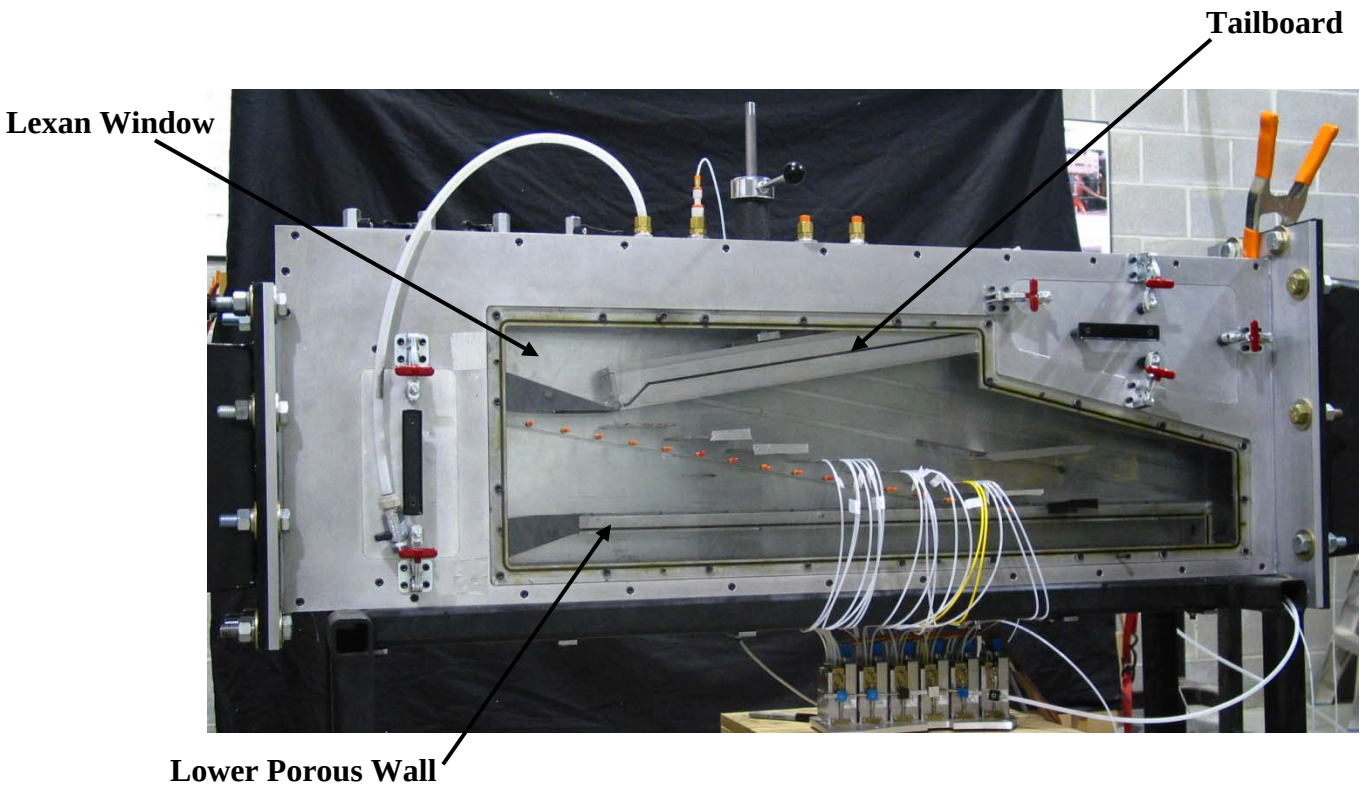

Figure E.4: Picture of GE Cascade

E.2.2 Test Section Instrumentation

The test section inlet conditions were measure with a single total pressure probe, 16 static pressure taps, and inlet Kiel probe traverses (Figure E.5). The single total pressure probe was mounted at mid span, 2 chord lengths in front of the fifth blade, approximately at the middle of the cascade. The static pressure taps were mounted at a distance of approximately 1 chord length in front of the cascade. They were spaced regularly in the pitch-wise direction at each mid passage and in front of each blade. The Kiel probe traverse was performed at a distance of approximately one chord length in front of the cascade. The span-wise location of the probe could be adjusted from one endwall to the opposite endwall. Traverse slots for an exit total pressure probe were

added for later tests.

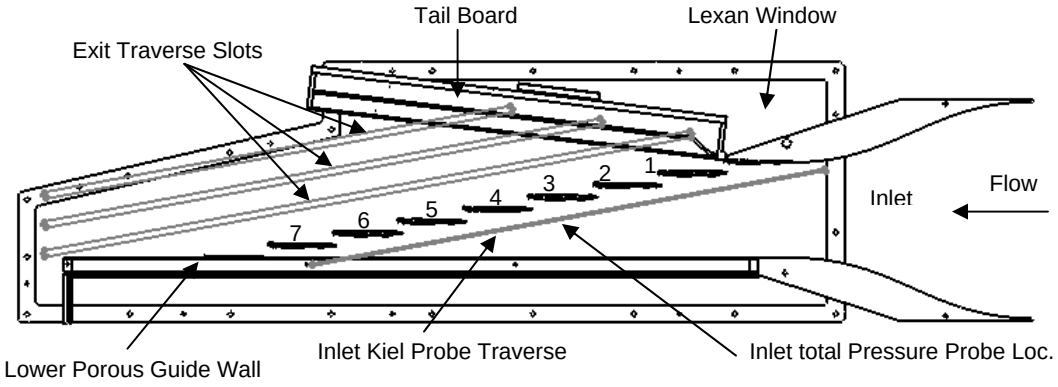

Figure E.5a: Traverse Slot Locations

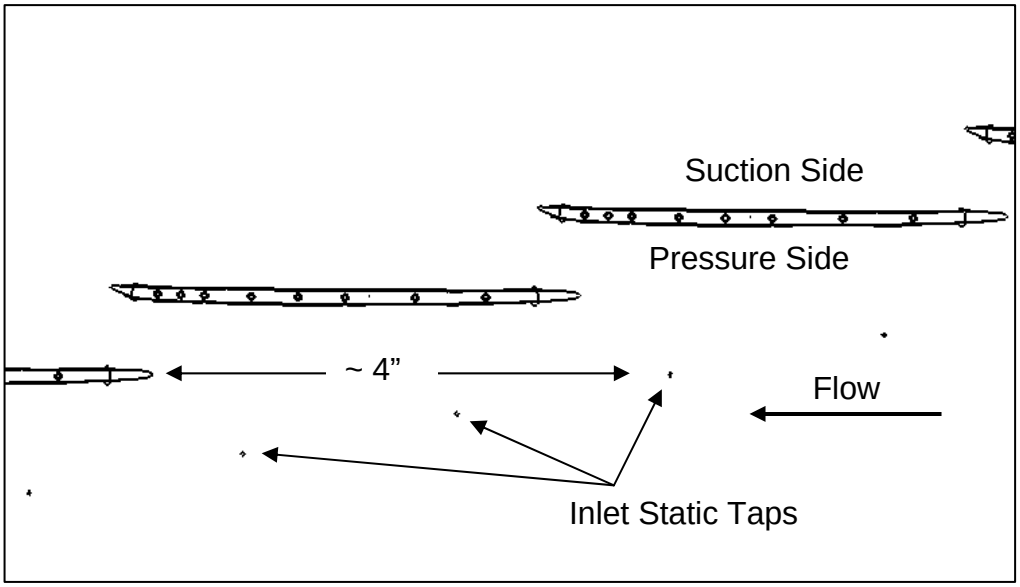

Figure E.5b: Static Pressure Taps

Three blades were instrumented with surface pressure taps on the suction and pressure sides. With limited space for pressure taps preference was given to the suction side due to the more complicated effects occurring there. Ten pressure taps were placed on the suction side and three were placed on the pressure side. The positions of these

pressure taps are shown in Table E.1 below. Due to variations in manufacturing Some blades were missing a pressure tap location, but all were capable of providing enough information to determine the periodicity of the flow. The interchangeability of the blades also allowed the missing pressure taps to be read by other blades.

Pressure Side Positions (% chord)	Suction Side Positions (% chord)
20	20
35	80
45	90
50	
55	
60	
65	
70	
75	
85	

Table E.1: Blade Pressure Tap Locations

Pressure measurements were acquired using 8 transducers with ±10psia range and 40 transducers with ±5psia range. These pressure transducers have an accuracy of ±.065%FS and were temperature compensated from 0°C to 50°C. Data was acquired using a LabVIEW [15] program designed to take data for a given period of time while the tunnel was in operation. The analog to digital conversion rate was 200khz, but the LabVIEW program averaged every four data points and recorded them.

E.2.3 Methods for Improving Periodicity

The test section was designed to accommodate many different methods for achieving periodicity. The four primary variations on the test section were to use a solid tailboard, a porous tailboard, no tailboard, and contoured tailboard. The solid tailboard

served as a baseline case where the expansion could be adjusted to create the proper pressure ratio and the shock structures could be observed. The porous tailboard was designed with adjustable porosity and various zones of pressure on the backside of the tailboard. The pressure zones could be adjusted with moveable dividers, and the pressure controlled using valves and tubing connected to downstream low pressure areas. Configurations using no tailboard were tested by using various amounts bypass air injected in place of the tailboard. This allowed the pressure of the air on the stagnant side of the free shear layer boundary to be controlled and the position of the free shear layer boundary to be controlled. The final configuration to be tested was the use of a contoured wall in place of the tailboard. The contoured wall was produced using CFD model to define the shape. Adjustments to this model were difficult since once produced the wall could not be reshaped.

E.3.0 Test Results

The GE air cascade was initially run with each tailboard configuration using only shadowgraphs to establish the effectiveness of each method in establishing periodic flow. Blade pressure measurements were then made on selected configurations based on the preliminary shadowgraph results. The first tests were run using a solid tailboard with static pressure taps along its midspan to measure the exit static pressures at various downstream distances. Measurements of the cascade pressure ratio (inlet total pressure/ tailboard exit static) were made with the tailboard set at different angles to establish the required angles for each pressure ratio tested. A tailboard angle of eleven degrees was found to produce the desired pressure ratio of seven. The shadowgraphs for this configuration showed a high aperiodicity in the flow (Figure E.6). Measurements of the

impact location of the pressure side fishtail shocks on the adjacent blade suction side and the suction side fishtail shocks quantified the aperiodicity (Table E.2).

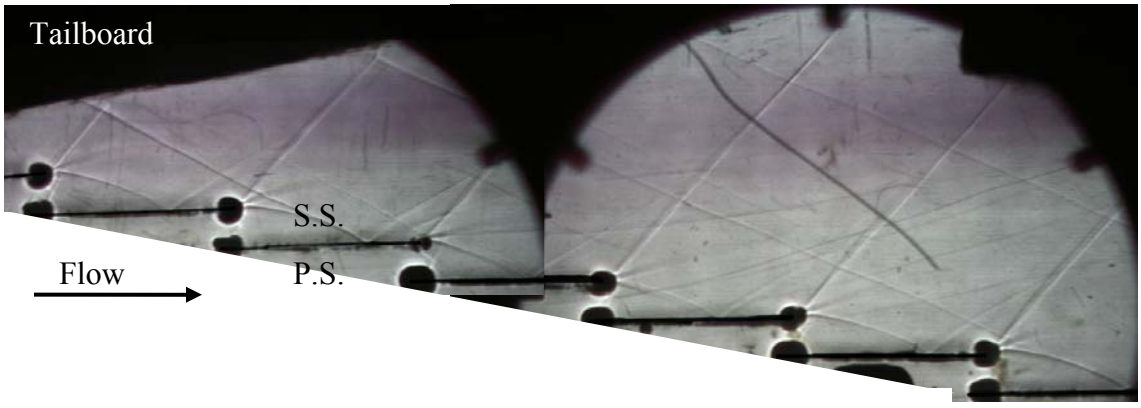

Figure E.6: Solid Tailboard Shadowgraph

	Suction Side Fishtail Shock Angle	Pressure Side Leg Impingement on Adjacent Blade
Blade 1	49.6	68%
Blade 2	47.4	73%
Blade 3	48.3	59%
Blade 4	48.0	60%
Blade 5	47.7	72%
Blade 6	49.0	75%

Table E.2: Solid Wall Shock Periodicity Data

The shadowgraphs show strong shock reflections from the solid tailboard that intersect the cascade again at roughly every third blade. These reflected shocks align themselves with the pressure side fishtail shocks of the blade immediately upstream of the blade they impinge on. As they combine with the fishtail shocks they increase the strength of the fishtail shock and negatively affect the periodicity. Also visible in the shadowgraph are faint double shock reflections from the solid tailboard that were

predicted in the CFD model (Figure E.7). Blade pressure measurements were made at a tailboard angle of ten degrees to quantify the aperiodicity (Figure E.8). It can be seen that there is a significant aperiodicity between the first blade and the rest of the cascade. It is also apparent that there is a great deal of aperiodicity between all blades near the trailing edge.

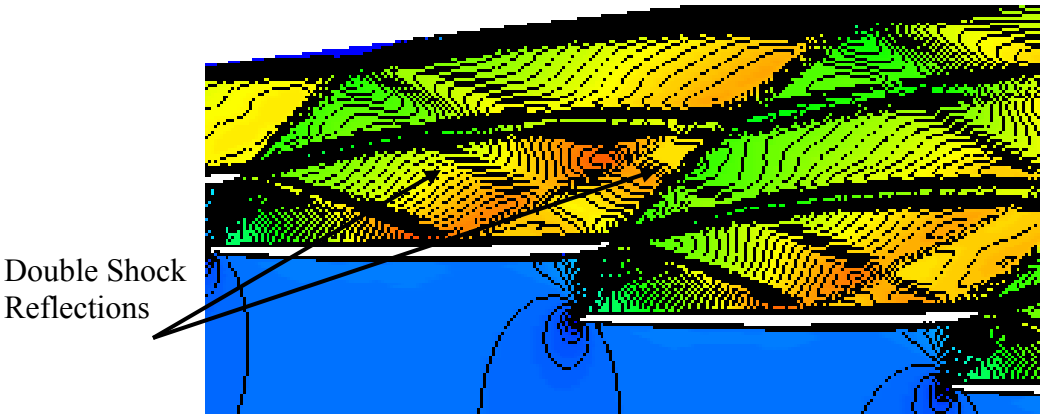

Figure E.7: CFD Predicted Double Shock Reflections

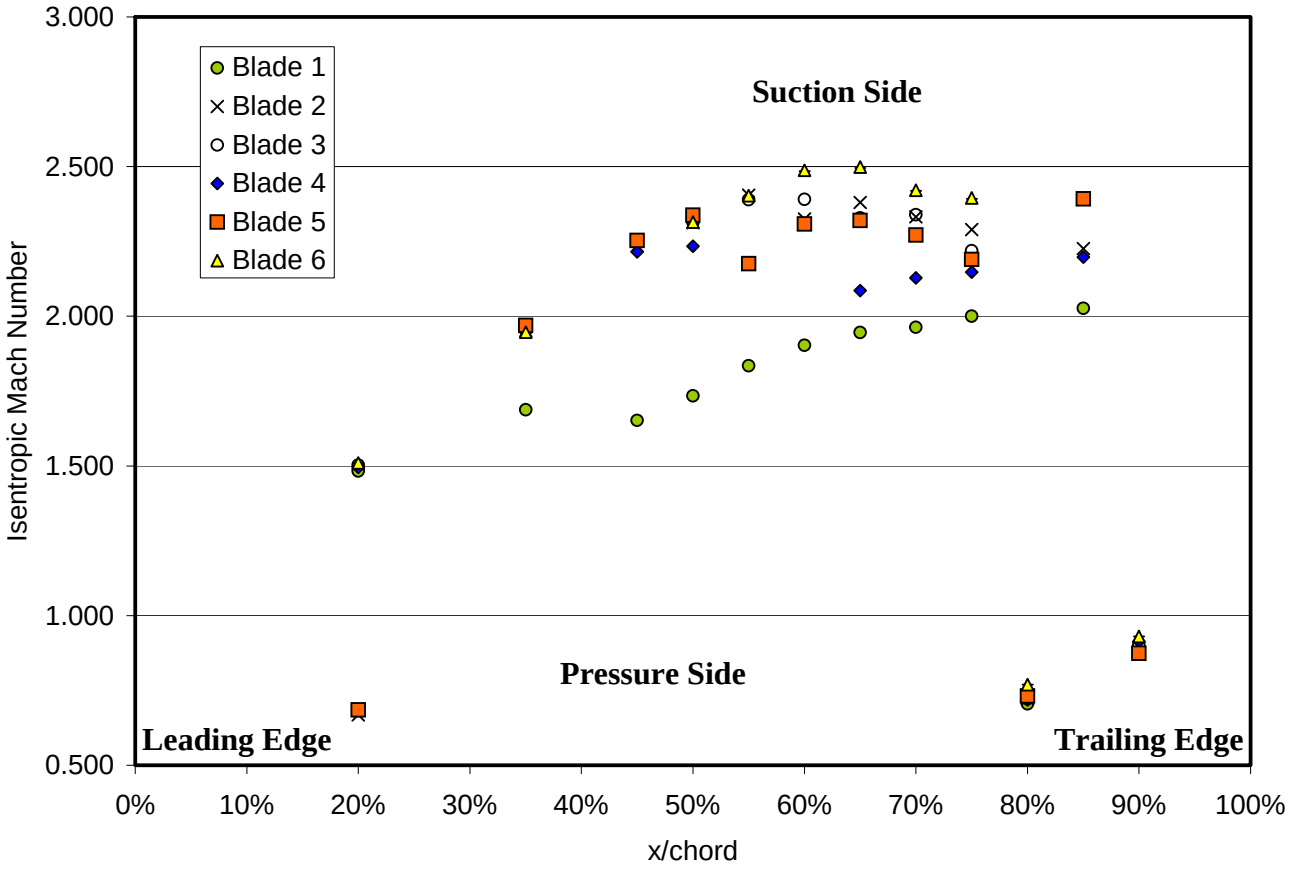

Figure E.8: Blade Surface Isentropic Mach Numbers for Solid Tailboard

E.3.1 Flow Visualization

Flow visualization was performed by coating a blade surface of the cascade with a mixture of silicon oil and powdered, fluorescent paint pigment. The mixture will not dry and when the tunnel is run the paint with flow over the surface of the blades driven by the shear of the air flow. This method will show zones of separation, reattachment locations, shock impingements, and endwall effects. Pictures of the blade were taken at close intervals while the tunnel was in operation to show the flow directions and the evolution of the secondary flow structures.

Flow visualization was performed on a blade from the GE air cascade to confirm that a sufficiently large zone of two dimensional flow existed at a span of three inches. A lower cascade blade with strong a strong shockwave impingement was selected. This flow visualization showed some interesting secondary flow features near the endwalls but the endwall influence was limited to 0.75 inches on each side leaving a sufficiently large 2-D flow section (Figure E.9).

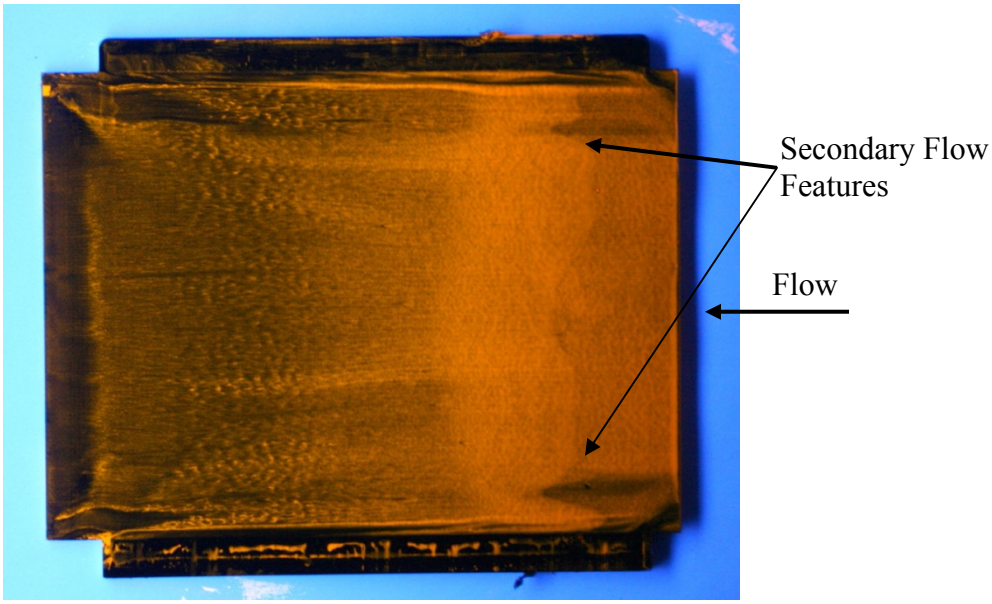

Figure E.9: Flow Visualization on Suction Side of Cascade Blade

E.3.2 Spanwise Total Pressure Data

Data was taken with the inlet total pressure traverse probe at different spanwise locations. This data showed that there was a large zone of constant inlet total pressure starting at approximately 0.5 inches off the endwall. The endwall boundary layer was larger for the lower cascade blades where the boundary layer had a much greater distance to develop (Figure E.10). The sidewall boundary layer had also grown much larger at the lower blades and contributed to the difference in total pressure. The total pressure for the

lower most blade in the cascade showed that the flow was unaffected at a distance of approximately 1 inch out from the side wall. The sidewall boundary layer made data from the lower most passage unusable and so a larger endwall boundary layer was acceptable here.

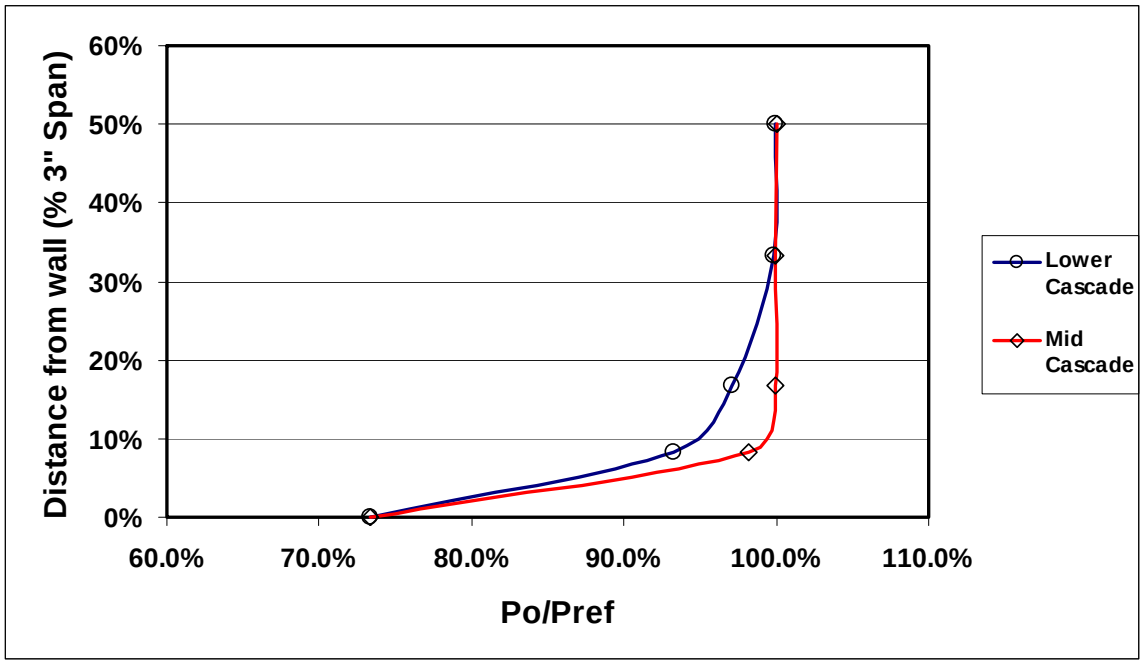

Figure E.10: Inlet Total Pressure Measurements in the Spanwise Direction

E.3.3 Porous Wall

The porous wall configuration was the first method tested for improving the periodicity. Compressible flow theory shows that if a shockwave reflects from a solid surface it will reflect as a shockwave, but if it reflects from a free shear layer between two fluids it will instead reflect as an expansion wave. The porous wall creates a mix of reflected shockwaves from the solid surfaces and expansion waves from the open holes that act like a free shear layer interface. If these two types of reflections are balanced properly the net result will be no reflected wave.

The porous wall was designed to have variable zones of controlled pressure on the back side of the porous plate. Porosity of the plate could also be adjusted to achieve the best shock reflection cancelation. The porosity was adjusted from 23% open to 0% (solid wall) open. The best cancellation of reflected shocks was found at 23% open. This best case cancellation of shock reflections was shown to greatly reduce the strength of the reflected shocks but did not eliminate them. The shadowgraph shows that reflected shocks are initially weak near the tailboard but strengthen as they approach the cascade (Figure E.11). Porous walls resulted in zones of air injection and suction on the tailboard boundary. The net movement of fluid through the wall seems to be responsible for the change in the fishtail shock angles. This resulted in lower periodicity which is quantified in the shock angles and impingement locations (Table E.3).

Changes in the distribution of pressure on the backside of the wall seemed to have little effect in cancelling the reflected shockwaves but did negatively affect the fishtail shock angles and result in reduced periodicity. Overall the porous wall method was not shown to be effective in cancelling shocks and blade surface pressure measurements were not taken. Additional work in refining the porosity of the walls, including adjustments to the void ratio, and adjustments to shape and size of the open spaces in the walls could result in better periodicity as shown by Paciorri and Rona [26-28], but these changes were beyond the scope of this investigation.

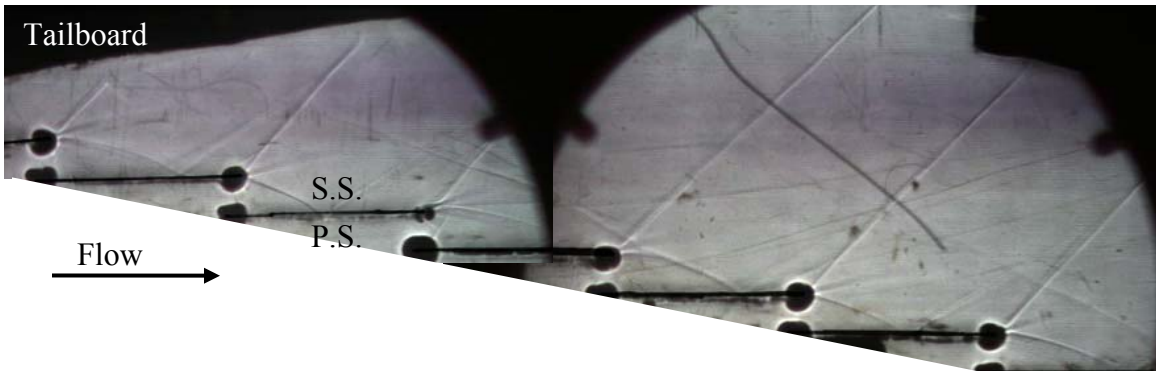

Figure E.11: Porous Wall Shadowgraph (23% Open)

	Suction Side Fishtail Shock Angle	Pressure Side Leg Impingement on Adjacent Blade
Blade 1	45.0	72%
Blade 2	49.0	52%
Blade 3	49.3	81%
Blade 4	44.4	68%
Blade 5	46.8	59%
Blade 6	46.8	67%

Table E.3: Porous Wall Shock Periodicity Data (23% Open)

E.3.4 No Tailboard

The next method for improvement of periodicity that was tested in the GE air cascade was to use no tailboard and allow the shockwaves to reflect off a free shear layer between stagnant air and the fast moving air exiting from the cascade. As mentioned in section 4.3 shockwaves intersecting a free shear layer will reflect as expansion waves instead. In theory these expansion waves will be weaker than shock waves but still pose a significant problem for the cascade periodicity. The CFD results for this model showed very poor periodicity in the cascade (Figure E.12). To improve this method it was desired that the pressure of the stagnant fluid be controllable. This was accomplished by allowing bypass air into the cascade above the free shear layer through control valves (Figure E.13). This meant that the air on the upper side of the free shear layer would be

moving as well and have a controlled pressure. It was hoped that this would better simulate an infinite cascade boundary by allowing the free shear layer to have a contour closer to that of the periodic flow condition. It was also hoped that it would reduce the strength of reflected expansion waves (Figure E.14).

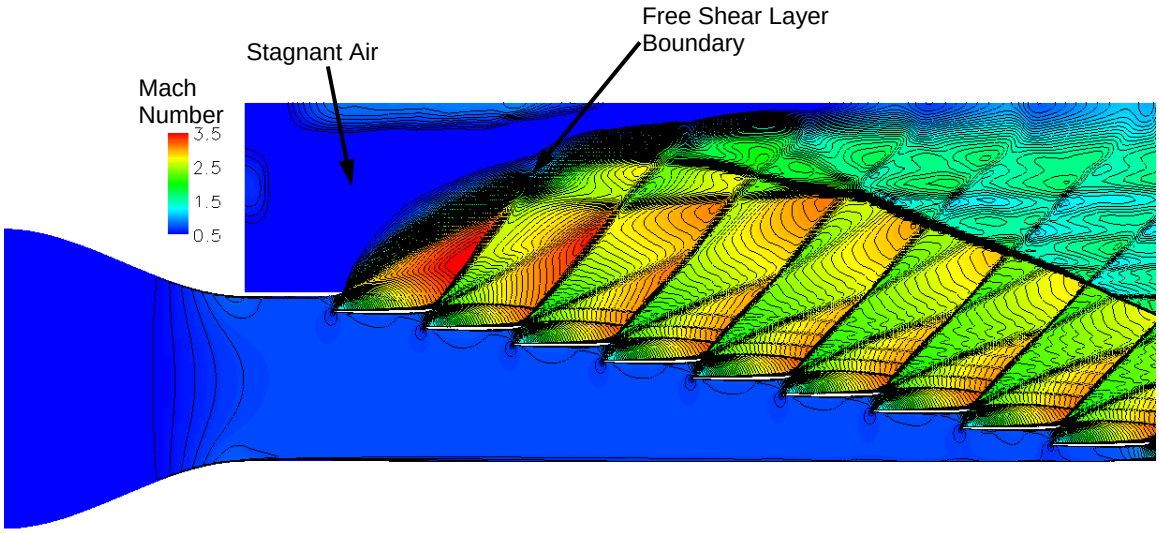

Figure E.12: CFD Results for No Tailboard, No Bypass Air

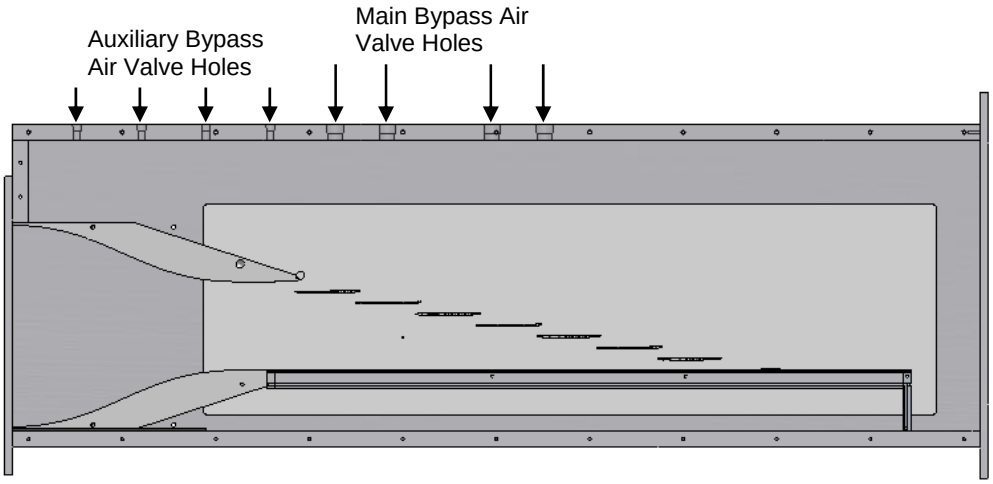

Figure E.13: No Tailboard Configuration Schematic

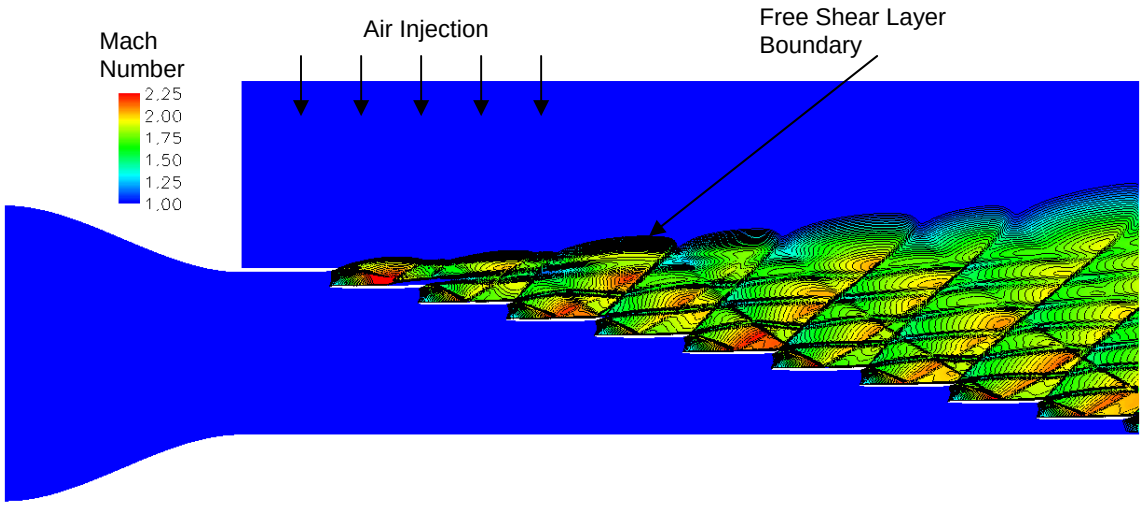

Figure E.14: CFD Results for No Tailboard with Bypass Air

The first trials with no tailboard were conducted with no bypass air allowed into the cascade. The shadowgraphs from these tests confirmed the CFD results and showed that the first passages were greatly over expanded (Figure E.15). This can be seen in the shadowgraph as curved pressure side fishtail shocks. It can be seen in this shadowgraph that the impingement location of the pressure side fishtail shock on the adjacent blade suction side occurs much further down stream than the periodic case. However the shock angles of the mid cascade blades showed improved periodicity. In a series of shadowgraph pictures taken during the test at several times a second, the fishtail shocks of the first two to three blades and the last blade are seen to be unsteady.

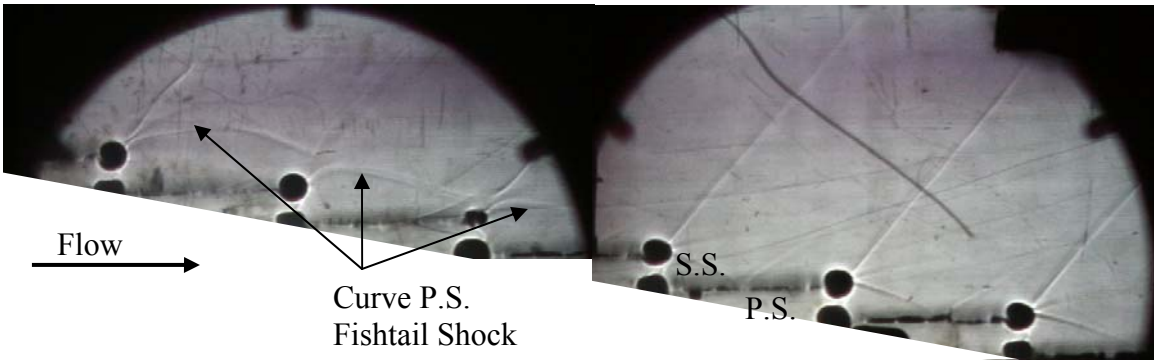

Figure E.15: No Tailboard, No Bypass Air Shadowgraph

Valves allowing air into the cascade were added to the test section to increase the number of blades achieving periodic conditions. Through a process of experimentation using various configurations of valve openings the most periodic conditions were found to be achieved with the 2 most upstream valves wide open, and the remaining valves closed. A shadowgraph of this configuration showed that one more nearly periodic passage was gained (Figure E.16). Opening the valves further down stream seemed to increase the unsteadiness of the fishtail shocks on the upstream blades. Opening these valves likely created concentrated jets of air which did not diffuse before intersecting the cascade. The measurement of the shock angles and impact locations from several shadowgraphs showed that blades 4-6 were the most likely to be periodic and steady (Table E.4). These blades were also found to be unsteady when blade surface pressure measurements were taken. The unsteadiness of the shockwave locations can be seen in Figure E.17 where the error bars show the range of pressure recorded during the test. The error bars for blade five can not be seen because they are significantly smaller.

This method showed improved periodicity in the cascade but did not achieve the levels of periodicity desired. To increase the periodicity it is recommended that a baffle

plate be added to diffuse the jets of air entering the cascade from the valves, and reduce the unsteady effects seen in the upstream blade fishtail shocks. However this addition to the cascade was outside of the scope of these tests and was not tested.

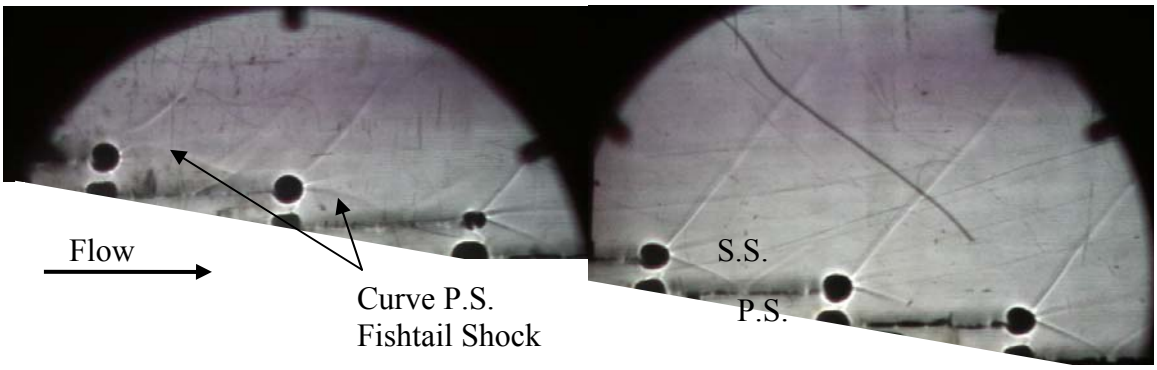

Figure E.16: No Tailboard, With Bypass Air Shadowgraph

	Suction Side Fishtail Shock Angle	Pressure Side Leg Impingement on Adjacent Blade
Blade 1	Unsteady	Unsteady
Blade 2	Unsteady	Unsteady
Blade 3	48.0	55%
Blade 4	50.6	54%
Blade 5	49.0	Unsteady
Blade 6	52.0	50%

Table E.4: No tailboard Shock Periodicity Data

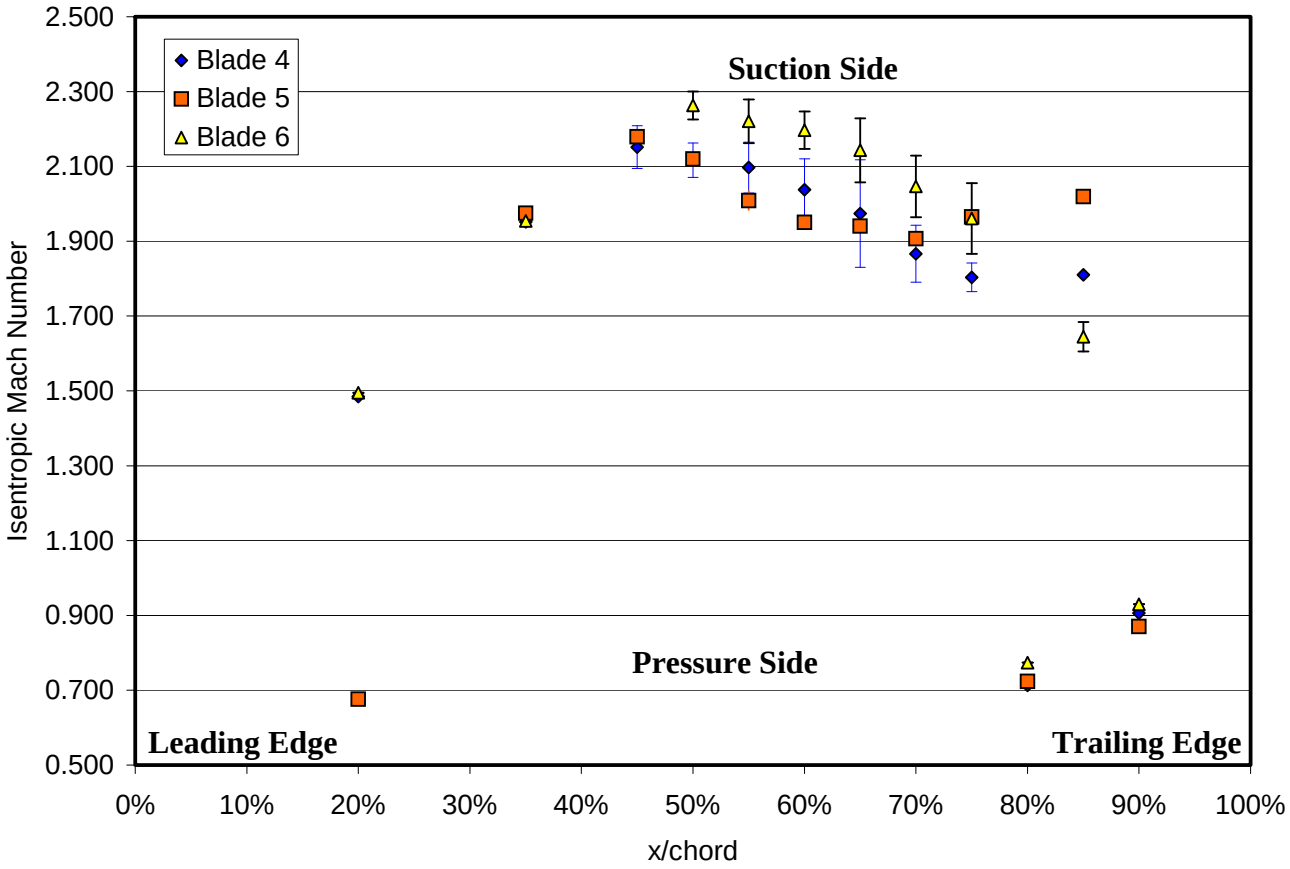

Figure E.17: No Tailboard Blade Surface Isentropic Mach Number

E.3.5 Contoured Tailboard

The final method tested for improving the periodicity of the cascade was to use a contoured tailboard. The shape of the contoured tailboard was determined by finding the streamlines for a periodic cascade and matching them with a shaped wall. The final design of the contoured wall was determined from a process of iteration where a design was checked using CFD and then redesigned based on the results. The final design showed improved periodicity in the CFD calculations (Figure E.18).

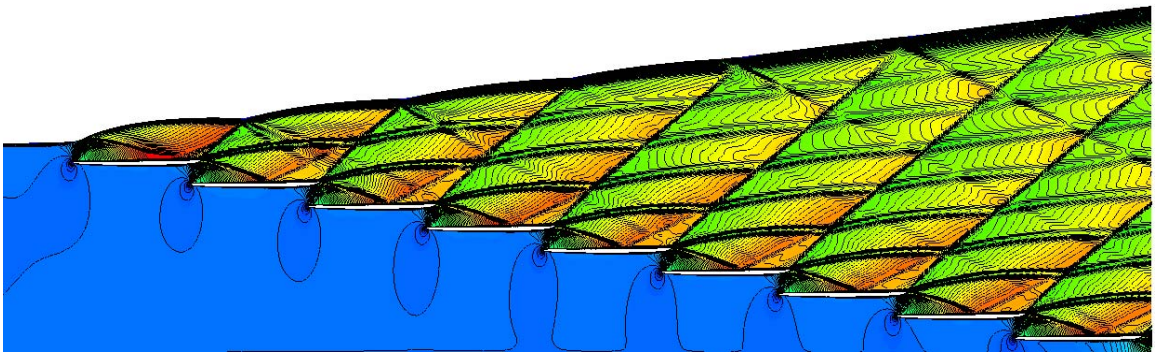

Figure E.18: CFD Results for Contoured Wall

Tests were conducted with the contoured tailboard set at several angles from 8.7 to 11 degrees. Changing the angle of the contoured tailboard was shown to change the impingement location from the reflected shockwaves and the pressure side fishtail shock. The effects of changing the tailboard angle were greatest on the fifth and sixth blades. The sixth blade was affected by the impingement of the reflected shockwave from the second blade fishtail shock. At tailboard angles of nine and ten degrees the reflected shock wave did not intersect the sixth blade producing better periodicity in the blades 4-6. The effects on the fifth blade seem to be due to a change in the location of the pressure side fishtail shock from blade four. Blade one was shown to be unaffected by the tailboard angle.

The best periodicity was found with the tailboard angle set to 10 degrees. This produced blade surface isentropic Mach numbers near those found with the straight tailboard set to ten degrees. The shadowgraphs for this angle show that the fishtail shock reflection from the second blade completely misses reintersecting the cascade producing better periodic conditions in blades 4-6 (Figure E.19). The effect on the third blade of the

impingement of the suction side fishtail shock reflection from the first blade was also reduced as can be seen in the blade surface isentropic Mach numbers (Figure E.20).

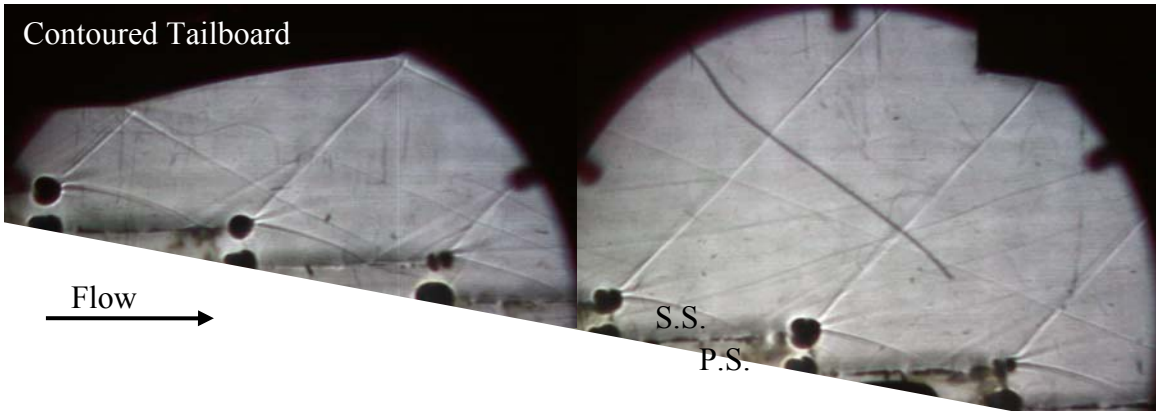

Figure E.19: Contoured Tailboard Shadowgraph (10 degrees)

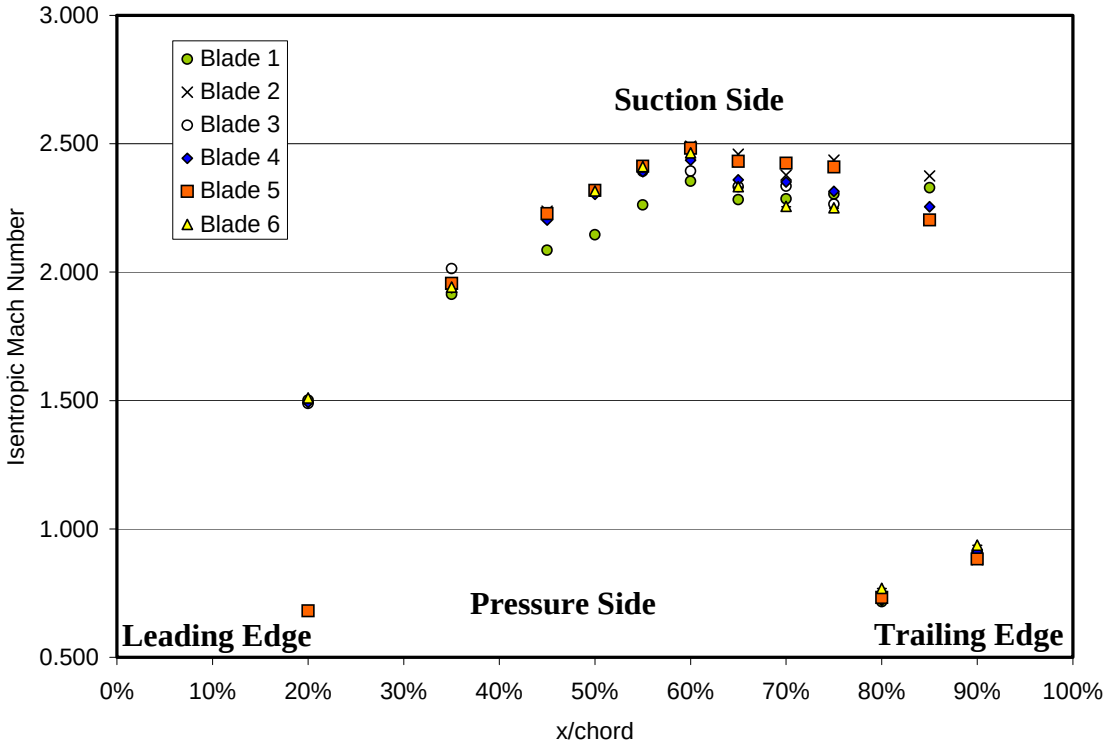

Figure E.20: Contoured Tailboard Blade Surface Isentropic Mach Number

E.4.0 Conclusion

The preliminary results of these air cascade tests showed that the size of the test section for the GE steam cascade facility could be greatly reduced. It was shown first that the aspect ratio for the facility could be reduced to 0.75 cutting the mass flow requirements in half from the original estimates. Second it was shown that the periodicity was not significantly improved beyond 8 passages. This will allow for the number of passages to be reduced from initial estimates. By using a contoured tailboard the periodicity can be improved enough to provide much improved test results. The net result of these modifications is a more periodic cascade requiring one third the mass flow initially estimated. This will greatly reduce the cost of building the GE steam cascade facility.

Literature Cited

1. Christie, D.G. and G.W. Hayward, *Observation of Events Leading to the Formation of Water Drops Which Cause Turbine Erosion.* Philosophical Transactions of the Royal Society of London Series A, Mathematical and Physical Sciences, 1966. **Vol. 260**(No. 1110): p. 183-192.
2. Moore, M.J., et al., *Predicting the Fog Drop Size in Wet Steam Turbines.* Inst. Mech. Engrs., 1973: p. 101-109.
3. Skillings, S.A., *Condensation Phenomena in a Turbine Blade Passage.* Journal of Fluid Mechanics, 1989. **200**: p. 409-&.
4. White, A.J., J.B. Young, and P.T. Walters, *Experimental validation of condensing flow theory for a stationary cascade of steam turbine blades.* Philosophical Transactions of the Royal Society of London Series a-Mathematical Physical and Engineering Sciences, 1996. **354**(1704): p. 59-88.
5. Bakhtar, F., H. Mashmoushy, and J.R. Buckley, *On the performance of a cascade of turbine rotor tip section blading in wet steam- Part 1: generation of wet steam of prescribed droplet sizes.* Proceedings of the Institution of Mechanical Engineers Part C-Journal of Mechanical Engineering Science, 1997. **211**(7): p. 519-529.
6. Bakhtar, F., H. Mashmoushy, and O.C. Jadayel, *On the performance of a cascade of turbine rotor tip section blading in wet steam - Part 3: wake traverses.* Proceedings of the Institution of Mechanical Engineers Part C-Journal of Mechanical Engineering Science, 1997. **211**(8): p. 639-648.
7. Bakhtar, F., H. Mashmoushy, and O.C. Jadayel, *On the performance of a cascade of turbine rotor tip section blading in wet steam- Part 2: Surface pressure distributions.* Proceedings of the Institution of Mechanical Engineers Part C-Journal of Mechanical Engineering Science, 1997. **211**(7): p. 531-540.
8. Bakhtar, F., S.Y. Rassam, and G. Zhang, *On the performance of a cascade of turbine rotor tip section blading in wet steam - Part 4: droplet measurements.* Proceedings of the Institution of Mechanical Engineers Part C-Journal of Mechanical Engineering Science, 1999. **213**(4): p. 343-353.
9. Ikeda, T. and A. Suzuki, *Some Findings on The Flow Behavior of Last Stage Turbine Buckets by Linear Cascade Tests in Steam.* 1972.
10. Parvizinia, M., et al., *Numerical and Experimental Investigations Into the Aerodynamic Performance of a Supersonic Turbine Blade Profile.* Proceedings of ASME Turbo Expo 2004, 2004.
11. The Mathworks, I., *Matlab R2007b*. 2007: Natick, Ma.
12. Kornhauser, A.K., *Personal Communication*, J. McFarland, Editor. 2007: Blacksburg, Va.
13. Moore, M.J. and C.H. Sieverding, *Two-phase steam flow in turbines and separators : theory, instrumentation, engineering*. Series in thermal and fluids engineering. 1976, Washington: Hemisphere Pub. Corp. xi, 399 p.
14. Johnson, R.W., *The handbook of fluid dynamics*. 1998, Boca Raton, Fla.: CRC Press. 1 v. (various pagings).
15. National Instuments. *http://www.ni.com*. 2008 12-10-2008].

16. Guha, A., *Nucleation, Droplet Growth And Condensation in Pure Steam Flows*, in *Two-phase flows with phase transition : May 29 - June 1, 1995*. 1995, von Karman Institute for Fluid Dynamics: Rhode Saint Genèse, Belgium. p. 1 v. (various pagings).
17. Kleitz, A. and J.M. Dorey, *Instrumentation for Wet Steam.* J. Mechanical Engineering Science Proc. Instn Mech. Engrs, 2004. **218**.
18. Albrecht, H.-E., *Laser doppler and phase doppler measurement techniques*. Experimental fluid mechanics. 2003, Berlin ; New York: Springer. xiii, 738 p.
19. Bakhtar, F., M. Ebrahimi, and R.A. Webb, *An Investigation of Nucleating Flows of Steam in a Cascade of Turbine Blading - Wake Traverses.* Journal of Fluids Engineering, 1994. **116**(March 1994): p. 121-127.
20. Estevadeordal, J., *PIV in Wet Steam*, S. Guilliot, Editor. 2008.
21. Bakhtar, F., H. Mashmoushy, and O.C. Jadayel, *Calibration characteristics of a three-hole probe and a static tube in wet steam.* International Journal of Heat and Fluid Flow, 2001. **22**(5): p. 537-542.
22. Moore, M.J. and C.H. Sieverding, *Aerothermodynamics of low pressure steam turbines and condensers*. 1987, Washington: Hemisphere Pub. Corp. xii, 290 p.
23. Guillot, S., *Personal Communication*, J. McFarland, Editor. 2007: Blacksburg, Va.
24. Aerosoft, I., *GASP v4*. 2008: Blacksburg, Va.
25. Gostelow, J.P., *Cascade aerodynamics*. 1st ed. Thermodynamics and fluid mechanics series. 1984, Oxford [Oxfordshire] ; New York: Pergamon Press. xvi, 270 p.
26. Paciorri, R., F. Sabetta, and A. Rona, *Wave reflection on porous walls: numerical modelling and application to transonic wind tunnels*, in *40th AIAA Aerospace Sciences Meeting and Exhibit*. 2002: Reno, NV.
27. Rona, A., et al., *Wall interference in the discharge ow in a linear cascade wind tunnel*, in *41st Aerospace Sciences Meeting and Exhibit*. 2003: Reno, Nevada.
28. Rona, A., et al., *Slot width augmentation in a slotted-wall transonic linear cascade wind tunnel*, in *42nd AIAA Aerospace Sciences Meeting and Exhibit*. 2004: Reno, Nevada.
29. Vicharelli, A. and J.K. Eaton, *Turbulence measurements in a transonic two-passage turbine cascade.* Experiments in Fluids, 2006. **40**(6): p. 897-917.